HAL
open science

On the possibility of recovering palaeo-diurnal magnetic variations in transitional lava flows: 2) An experimental case study

Christian Vérard, Roman Leonhardt, Michael Winklhofer, Karl Fabian

To cite this version:

Christian Vérard, Roman Leonhardt, Michael Winklhofer, Karl Fabian. On the possibility of recovering palaeo-diurnal magnetic variations in transitional lava flows: 2) An experimental case study. Physics of the Earth and Planetary Interiors, 2008, 169 (1-4), pp.117. 10.1016/j.pepi.2008.07.018 . hal-00532165

HAL Id: hal-00532165

https://hal.science/hal-00532165v1

Submitted on 4 Nov 2010

HAL is a multi-disciplinary open access archive for the deposit and dissemination of scientific research documents, whether they are published or not. The documents may come from teaching and research institutions in France or abroad, or from public or private research centers.

L'archive ouverte pluridisciplinaire **HAL**, est destinée au dépôt et à la diffusion de documents scientifiques de niveau recherche, publiés ou non, émanant des établissements d'enseignement et de recherche français ou étrangers, des laboratoires publics ou privés.

Accepted Manuscript

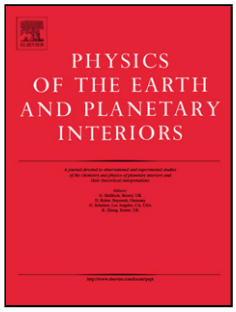

Title: On the possibility of recovering palaeo-diurnal magnetic variations in transitional lava flows: 2) An experimental case study

Authors: Christian Vérard, Roman Leonhardt, Michael Winklhofer, Karl Fabian

PII: S0031-9201(08)00181-7
DOI: doi:10.1016/j.pepi.2008.07.018
Reference: PEPI 5012

To appear in: *Physics of the Earth and Planetary Interiors*

Received date: 15-2-2008
Revised date: 11-7-2008
Accepted date: 12-7-2008

Please cite this article as: Vérard, C., Leonhardt, R., Winklhofer, M., Fabian, K., On the possibility of recovering palaeo-diurnal magnetic variations in transitional lava flows: 2) An experimental case study, *Physics of the Earth and Planetary Interiors* (2007), doi:10.1016/j.pepi.2008.07.018

This is a PDF file of an unedited manuscript that has been accepted for publication. As a service to our customers we are providing this early version of the manuscript. The manuscript will undergo copyediting, typesetting, and review of the resulting proof before it is published in its final form. Please note that during the production process errors may be discovered which could affect the content, and all legal disclaimers that apply to the journal pertain.

* Manuscript
ACCEPTED MANUSCRIPT

On the possibility of recovering palaeo-diurnal magnetic variations in transitional lava flows: 2) An experimental case study.

Christian Vérard[1], Roman Leonhardt[2], Michael Winklhofer, Karl Fabian[3]

Ludwig – Maximilians – Universität, Department für Geo- und Umweltwissenschaft, Geophysik Bereich, 80333 MÜNCHEN, DEUTSCHLAND.

1 – Now at the Faculté des Géosciences et de l'Environnement, Institut de Géologie et Paléontologie, Université de Lausanne (UNIL), Quartier Dorigny, 1015 Lausanne, SWITZERLAND.
2 – Now at the Department for Applied Geosciences and Geophysics, Montan University, 8700 Leoben, AUSTRIA.
3 – Now at the Geological Survey of Norway, NGU, Trondheim, NORWAY.

Abstract

Geomagnetic field variations of external origin may be enhanced during periods of transitional field behaviour, particularly when the dipole moment is low, in which case they are likely to leave a paleomagnetic signature in rapidly cooled lava flows. To test this proposition, we have resampled en bloc and studied in fine detail a thin transitional Aa flow from a mid-Miocene lava sequence on Gran Canaria which was paleomagnetically investigated previously (Leonhardt & Soffel, 2002). The flow is characterised by high-unblocking temperatures, an equatorial VGP position and a very low absolute palaeointensity of ~2 µT. Two slabs were cut out of the flow and sampled at 1 cm intervals, along four vertical profiles running parallel to each other. Thermal demagnetisation was performed on two profiles using heating steps as small as 15°C at elevated temperatures. The high-temperature part of the unblocking spectrum was found to be remarkably constant across the flow, as was the Curie temperature of 540°C, and the negligible anisotropy of magnetic susceptibility. The exsolution lamallae observed under the microscope point to deuteric (high temperature) oxidation having occurred prior to the acquisition of the primary thermoremanent magnetisation. While the absolute palaeointensity values vary only little with vertical position, the magnetisation directions recovered by thermal demagnetisation vary considerably (on average, by some 20° at 500°C). These large variations

Accepted Manuscript

ACCEPTED MANUSCRIPT

can be attributed to an overprint by secondary minerals, formed by fluid diffusion around vesicles and low-temperature oxidation. Since the secondary magnetisation recorded transitional directions as well, the overprint must have occurred soon after emplacement. The directional variations typically decrease in amplitude with increasing blocking temperature, which is contrary to what would be expected if pronounced diurnal external field variations were trapped in the flow.

Keywords: Earth's magnetic reversal, palaeodirection, palaeointensity, magnetic mineralogy, external geomagnetic field variation.

Accepted Manuscript

ACCEPTED MANUSCRIPT

1. Introduction

Field variations of external origin have not attracted much attention in palaeomagnetic research so far. Not for the lack of interest, but simply because their relative contribution under normal field conditions is too small to be detected palaeomagnetically. Even during intense magnetic storms, the largest ground field perturbations of external origin do barely exceed 1 μT (at high geomagnetic latitudes) against a background field of 25-60 μT. Besides, such events do not occur frequently enough and it would be coincidence if a lava flow was cooling through the blocking temperature in the very instant of a sudden magnetic storm commencement. However, the situation may be different in times of a diminished main field with transitional geometry (Siscoe & Crooker, 1976; Ultré-Guérard & Achache, 1995). External variations are indeed expected to be significantly reinforced during periods of equatorial dipole fields. Under these circumstances, the magnetosphere reconfigures on diurnal time scales (Saito *et al*., 1978; Ziegler *et al*., 2004), leading to highly dynamic phenomena such as magnetic storms, which under normal field conditions are only observed during periods of increased solar activity. In our companion paper (Winklhofer *et al*., *this issue*), we show that enhanced diurnal external field variations superimposed on a weakened main field would leave a palaeomagnetic signature in a rapidly cooled thin lava flow. Thicker flows, cooling on time scale of months, efficiently smooth out diurnal external variations. Furthermore, it is one thing to have such variations recorded in a flow, it is quite another one to extract them palaeomagnetically, which requires a specialised sampling technique and an elaborated measurement protocol.

To begin with, a suitable candidate flow is needed. First, the flow must have been emplaced during low-intensity transitional field conditions. Then it needs to be thin enough (~50 cm thick) to cool off rapidly, as the cooling rate limits the temporal resolution when recording time-dependent signals. Ideally, the thermoremenance carriers should be pristine magnetic single-domain (SD) particles with blocking temperatures starting just below the Curie temperature. The absence of secondary overprint is not strictly required, provided that the overprint has low unblocking temperatures. These requirements

ACCEPTED MANUSCRIPT

reduce the choice of suitable lava flows drastically, and require a great deal of preliminary palaeo- and rock-magnetic reconnaissance studies.

Palaeomagnetic investigations carried out by Leonhardt & Soffel (2002) and Leonhardt *et al*. (2002) in the Canary Islands covered a composite section of a ~300 m thick lava pile in the mid-Miocene shield basalt of Gran Canaria. The study revealed, in particular, the presence of two excursions and one reversal interpreted to mark the beginning of polarity chron C5ACN (*i.e.* 14.1 Ma after Cande & Kent, 1995). For the present study, we selected one particular lava flow of the sequence that meets most of the above conditions besides alteration. Rather than taking oriented cores in the field, we cut out oriented block samples from this specific flow. The two blocks obtained were densely sampled at the laboratory, which allowed us to minimise the directional error between different samples within a block. We conducted detailed palaeo- and rock-magnetic investigations on all samples in an attempt to distinguish between systematic directional variations of external origin and magnetic overprints.

2. Sampling and methodology

The lava flow selected for the present investigations corresponds to site C-TP62 of Leonhardt & Soffel (2002). It is characterised by a transitional paleofield direction (Declination, D: 072.4° / Inclination, I: -04.8°) and a very low palaeointensity value of 1.2 ±0.5 µT. The virtual geomagnetic pole (VGP) plots near India, and is preceded by 15 flow units, which record a VGP cluster close to South America. The selected flow consists of olivine basalt of 'aa'-type, and is approximately 1 m thick including top and bottom breccias. A portable gasoline-powered diamond saw was used to cut two sub-vertical blocks, approximately 3 m apart from each other, out of the massive part of the flow. The top and bottom breccias were too friable to be sampled in this way. The blocks were orientated in the field (344.233°E; 27.936°N) using magnetic and sun compasses, and corrected for local declination (-7.1°).

Block.I is ~40 cm high and shows macroscopically four zones from bottom to top (Fig.1.A): a reddish, friable and oxidised zone from 0 to ~5 cm, a lower zone from 5 to ~15 cm showing relatively fine vesicles (millimetric), an upper zone from 15 to ~37 cm with relatively large vesicles (sub-

ACCEPTED MANUSCRIPT

centimetric), and finally a more and more friable but not necessarily oxidised zone up to 40 cm. Note also that the rock is broken at ~22 cm.

Block.II is similar in a height of ~47 cm and composed of similar zones (Fig.1.B). A 6-7 cm oxidised zone is present at the base of the flow, and a friable zone, close to the top breccia between 40-42 and 47 cm. A change in vesicle size is not obvious, but a distinction may be observed at about 20 cm between a lower and an upper zone. A severe break in the rock occurs between 33 and 35 cm, but another exists at 27 cm and some cracks appear at 12-13 cm and perhaps 22 cm.

An ~8 mm thick slice was cut again in each block at the laboratory (University of Munich), hereinafter referred to as slab.I & slab.II, and a 1 cm grid was marked throughout each slab surface. Four columns of cores were drilled every centimetre: one column of ~ 4 mm diameter cores and three columns of ~8.5 mm diameter cores further referred to as profiles A, B and C.

The smaller cores (~4 mm) were used for magnetic mineralogy analysis by means of a Petersen's Variable Frequency Translation Balance (VFTB) housed at the laboratory of Munich (Germany). The samples were subjected to measurements of hysteresis loops, isothermal remanent magnetisation (IRM) acquisition, backfield and thermomagnetic curves. Data were treated with the RockMagAnalyser 1.0 software (Leonhardt, 2006).

Cores from profiles A and C are used for the determination of the palaeodirections, and palaeointensities were determined from profile B. The anisotropy of magnetic susceptibility (AMS) was measured using a Kappabridge susceptibility-meter (KLY-2; 15 positions) on samples from profile A prior to demagnetisation. The shape of the ellipsoid of magnetic susceptibility (a quasi-sphere at more than 99.5%; Tauxe, 1998) and the degree of anisotropy (P_J < 1.01; Jelinek, 1981) indicate that the magnetic fabric of all samples from both blocks is quasi-isotropic. Palaeodirections were defined by thermal demagnetisation (20 steps; rest field in the oven <7 nT) on orthogonal projections (Zijderveld, 1967) using principal component analysis (PCA; Kirschvink, 1980) and on stereographic projections ("Schmidt" equal area). Palaeointensities were estimated using the Modified-Thellier Technique MT4 (Leonhardt *et al*., 2004a), which includes "pTRM*-tail checks" (Riisager & Riisager, 2001) and "additivity checks" (Krása *et al*., 2003). By combining these two last checks, it is

ACCEPTED MANUSCRIPT

possible to distinguish whether any significant deviation from the ideal behaviour is caused by multi-domain (MD) bias or by alteration. If no MD bias is detected and the thermo-remanence magnetic (TRM) properties are preserved as monitored by "additivity checks", a correction from alteration can be performed following the method proposed by Valet *et al*. (1996) and Leonhardt *et al*. (2003). Palaeointensity experiments were carried out with a MMTD-20 thermal demagnetiser and a laboratory-built sample holder for ~8.5 mm cores. For partial thermo-renanent magnetisation acquisition (pTRM/TRM), a magnetic field of 20 µT was applied during heating and cooling. Data analysis was performed with the ThellierTool 4.11 software (Leonhardt *et al*., 2004a) and its default reliability parameters. All directional and paleointensity measurements were carried out with a 2G-Cryogenic Magnetometer operating in the magnetically shielded room at the Niederlippach laboratory (University of Munich).

In addition to the magnetic measurements, four polished sections per slab (section surfaces of 2.5 cm diameter) have been examined using reflected light microscopy. Porosity and permeability measurements have been carried out on specific samples (2.5 cm in diameter, and 5 to 7 cm in length) drilled in the two blocks, from which also slabs.I and .II were cut out, respectively. Four samples were taken at about 2, 9, 15 and 30 cm (samples centre) in slab.I, and three at about 11, 33, and 42 cm in slab.II.

Open porosity was measured using a micrometrics AccuPyc 1330 porosimeter. Porosity varies from less than 12% in the lower zone to more than 35% in the upper zone of the two blocks. Note that the open porosity for the sample situated at about 9 cm from the bottom of slab.I was rising from 14% up to 33% after 1 hour heating at 300°C, due to the destruction of zeolite. Without the infill of vesicles, the open porosity appears to correspond, therefore, to approximately a third of the rock throughout the blocks.

Permeability to gas was determined using an autoclave developed by the laboratory of mineralogy (Munich, Germany) and following the measurement techniques of Müller *et al*. (2005). Only 50% of the gas (argon) at 15 bars went through the most permeable sample (slab.I-30; 30 cm) after 20 minutes, and still 90% of the gas remained blocked by the most impermeable sample (slab.I-09; 9 cm)

ACCEPTED MANUSCRIPT

after 45 minutes. These results indicate that the lava flow is quite impermeable. Nevertheless, the permeability may have been much higher and may have strongly decreased after percolation of a fluid and precipitation of zeolite (analcime) in the vesicles. Provided that zeolite is associated with the degassing of the lava flow itself, however, later fluids (or gas) might have circulated through the rock, but probably would have been restricted to cracks or failures zones and would have not percolated through the vesicles.

3. Magnetic mineralogy

3.1. Slab.I

The bulk susceptibility (Fig.1.$_A$), inferred from AMS measurements, shows relatively high values (~300×10^6 SI) for samples from the 12-13 first cm in slab.I, and a decrease between 13 and 16 cm, with susceptibility values of about 150 to 200×10^6 SI in the upper part of the profile. The decrease, in good correspondence with the change in vesicle size, is not related to a lack of material associated with larger vesicles in the upper zone, because the decrease in susceptibility values persists when data are normalised to samples mass (from 250×10^6 SI in the lower zone to 100×10^6 SI in the upper zone). Furthermore, this change is also found in terms of saturation magnetisation (M_S and M_{RS}). The value of M_S, for instance, increases rapidly in the basal oxidised zone (from 0.2 Am²/kg to 0.8-1.0 Am²/kg) to reach a rather constant value of 0.7-0.8 Am²/kg in the lower zone, before decreasing down to 0.4-0.5 Am²/kg in the upper zone and to as little as 0.3 in the top friable zone.

By contrast, coercivity values (B_C and B_{CR}) are relatively constant throughout slab.I with only a slight reduction towards the top (from 50 mT at 5 cm down to 43 mT at 40 cm for B_{CR}, for instance). Noticeably smaller values are found in the 5 first centimetres of the oxidised zone (B_{CR}=30 mT for the 2 first cm). The “anomalously low” value of the coercivity at 22 cm corresponds to a fracture in the rock.

ACCEPTED MANUSCRIPT

The major part of the lava flow is characterised by a single inflection point at 540°C in the thermomagnetic heating curve (high field=170 mT), consistent with a Curie temperature of titanium-poor (7-8%) titanomagnetite. Measurements in low field (14 mT), however, show an increase in magnetisation by heating between approximately 200° and 300°C, suggesting the wide presence of (titano-)maghaemite (Fig.2.$_A$). Both high field and low field thermomagnetic curves are irreversible witnessing the inversion of (titano-) maghaemite during thermal treatment.

Towards the basal part of the flow, in the lowermost 5 cm, two inflexions in the thermomagnetic heating curves indicate two distinct Curie temperatures: 480°C and 600°C. The temperatures are very similar whether they are defined from the peak in the second derivative (maximum curvature, e.g. Tauxe, 1998) or the Moskowitz's method (Moskowitz, 1981). Cooling curves are characterised by inflection points around 480°C throughout the profile.

Ore microscopy indicates the presence of exsolved titanomagnetite grains (Fig.2.$_B$), which witness the occurrence of high temperature deuteric oxidation (interpreted to be of class 3 in the classification of Ade-Hall *et al*., 1971). Moreover, such lamellae are not found in the oxidised zone of slab.I (5 first cm), which is further marked by a deep red colour, interpreted to be the sign of low temperature oxidation in addition to the high temperature oxidation. In the upper zone, mainly grains located in the vicinity of vesicles, predominantly filled up with zeolite, exhibit a reddish colour (Fig. 2.$_B$; 19-22 cm). The very occurrence of altered (oxidised) grains around vesicles is interpreted as a chemical reaction (oxidation) between the material contained in the vesicles and the nearby matrix of the rock. Otherwise, the matrix appears quite fresh. The fact that the lower zone is altered (oxidised) to a larger degree may be understood as a consequence of a larger contact area, because vesicles of the lower zone are finer but more numerous.

In summary, ore microscopy and thermomagnetic investigations point to the presence of low Ti-titanomagnetite within the matrix, dominating the magnetic behaviour of the lava flow, except for the lowermost part. Nevertheless, secondary titanomaghaemite is present, in particular, in the lowermost part of the slabs and close to vesicles.

ACCEPTED MANUSCRIPT

Hysteresis data are dominated by SD behaviour and points to a quite homogeneous distribution in magnetic grain size and domain state in the slab. Outlying data, plotting in the pseudo-single domain (PSD) range of the Day plots (Day *et al*., 1977), correspond to samples from the basal oxidised zone and from where the rock is broken.

3.2. Slab.II

Surprisingly, some magnetic properties of slab.II vary in a way markedly different from those of slab.I (Fig.1.$_B$). In slab.I, two zones with different vesicle size (section 3.1) were clearly reflected by the zoning in both susceptibility and saturation magnetisation. In slab.II, by contrast, it is the zoning in the coercivity values that mainly reflects the zoning in vesicle size.

The bulk susceptibility is lower in the lower zone with values in the order of 800×10^6 SI, and progressively increases from 18 cm, where a change in vesicles size was delimited (section 2), to values of 1400 to 2000×10^6 SI in the upper zone, before decreasing again in the top friable zone. "Anomalously low" values are clearly visible at 33-35 cm where the rock is severely broken. The increase at the boundary between lower and upper zones persists if the data are normalised to the mass, and is also observed in terms of saturation magnetisation (M_S and M_{RS}), but in a relatively smoothed manner. Values of M_S, for instance, range from 0.7 to 1.0 Am²/kg in the basal oxidised zone, decrease to 0.4 to 0.6 Am²/kg in the lower zone, and gradually increase from 18 cm up to 0.7-1.0 Am²/kg in the upper zone, except for samples close to the fracture (32-33 cm) where values are as low as 0.1 Am²/kg. The values of B_{CR}, by contrast, are close to 25-30 mT in the oxidised zone (6 first cm), increase sharply to 50 mT in the lower zone (7 to 17 cm), decrease as sharply down to 35 mT in the upper zone (20 to 38 cm), and finally increase gently towards to the top (~45 mT at 45 cm) in the friable zone. The analysis of Curie temperatures in slab.II is similar to those obtained for slab.I, although only one inflexion in the thermomagnetic curves was isolated. Curie temperatures are close to 620°C at the base of the slab, but decrease rapidly (in the 5-7 first cm) to a rather constant value of 540°C throughout slab.II, identical to that observed in slab.I. Thermomagnetic measurements and ore

ACCEPTED MANUSCRIPT

microscopy indicate that titanium-poor titanomagnetite is the main magnetic carrier as in slab.I, although (titano-)maghaemite is equally present.

The analysis of hysteresis parameters exhibits identical characteristics as those observed for slab.I, although data are slightly more elongated and show two clusters corresponding to the lower (smaller grains) and upper zones (larger grains) in slab.II.

4. Palaeomagnetic results

4.1. Palaeodirections from slab.I

When all thermal demagnetisation curves are placed next to one another according to the position of the samples in the slab, a "thermal demagnetisation surface" is obtained. The first derivative of this surface is a map of the unblocking temperature spectra throughout the different profiles (Fig.3). Three maps for slab.I, corresponding to the three profiles (A, B, and C), show a remarkably homogeneous unblocking spectrum in the interval between 500°C and 540°C, *i.e.* close to the Curie temperature. Only a few samples, which correspond to the oxidised zone or to fractures in the rock, depart from this behaviour.

From the variations in the rock-magnetic properties, such a homogeneous unblocking spectrum cannot be expected, all the more so, because the directions of magnetisation turn out to be very heterogeneous. Three components of magnetisation can be isolated from orthogonal projections (Fig.4.$_A$) after removal of a minor viscous magnetisation at 80°C: i) a low temperature component, C_{LT}, can be defined from 80° to 240°C; ii) a mid temperature component, C_{midT}, from 330° to 450°C; and iii) a high temperature component, C_{HT}, stable from 480-500° to 565°C. Overlaps of unblocking temperature spectra lead to the curvature of the different components, which renders their isolation sometime difficult.

When the directions of magnetisation are represented on a stereographic projection, components C_{LT} from samples of profiles A and C are scattered, due to the difficulty of clearly isolating these

ACCEPTED MANUSCRIPT

components. Nevertheless, the overall mean direction is D:051.0° / I:39.8° (α_{95}=7.2°; κ=9.78; N=45). The mid temperature components C_{midT} plot along a great circle, which has a pole-to-plane orientation of D:253.6° / I:63.4° (α_{95}=5.5°; κ=n/a; N=67). Finally, the high components C_{HT} are also widely distributed along the horizontal with an overall mean direction D:101.5° / I:-05.1° (α_{95}=4.2°; κ=16.74; N=74; the peak density is oriented: 090.3° / -02.9°).

The VGPs for C_{HT} fall near the equator in the Indian Ocean (Fig.6), with a pole position $HT._I$: longitude, ϕ=071.07° / latitude, λ=-11.35° (with semi-axes of the confidence ellipse: dp=2.09° / dm=4.16°). The VGPs inferred from the components C_{midT} are inevitably distributed along a great circle, but two clusters arise. One pole (cluster 1) is situated in Kirghizstan ($midT._I.c_1$: ϕ=079.25° / λ=38.43°; dp=5.45° / dm=10.12°) and the second (cluster 2) in Madagascar ($midT._I.c_2$: ϕ=048.74° / λ=-22.89°; dp=2.58° / dm=4.95°). The mean pole for C_{LT} falls north from the Aral See, below 60° in latitude ($LT_{2.3}$: ϕ=068.87° / λ=43.89°; dp=5.18° / dm=8.62°). These results imply that all directions of magnetisation do not correspond to a stable position of the dipolar field, and are thought to be related to the "El Paso" Earth's magnetic reversal recorded in the lava sequence from Gran Canaria (Leonhardt & Soffel, 2002).

It is of particular interest to look at the directions of the high temperature component C_{HT} according to the position of samples in the slab ($Fig.7._A$). At first glance, the two curves (from profiles A and C) look similar. However, in details, there are large discrepancies, in particular, in terms of declination. The most spectacular examples are found just at the level where a change in vesicles size occurs. In the most extreme case, at 18 cm, the declination observed in sample from profile C is D:069.3° (maximum angular deviation, MAD=12.1°), while in sample from profile A, D:126.9° (MAD=4.5°). It is a ~58° difference for two samples separated by only 2 cm. Discrepancies exist further up in the slab. Although the declinations are similar in profiles A and C at 27 cm ($D._A$: 107.1° / MAD=6.2°; $D._C$: 106.7° / MAD=9.6°), they are significantly different from samples in profiles A and C at 28 cm ($D._A$: 087.1° / MAD=7.7°; $D._C$: 082.5° / MAD=13.6°). It is a variation of more than 20° in 1 cm.

ACCEPTED MANUSCRIPT

4.2. Palaeointensities from slab.I

The ThellierTool 4.11 software (see Leonhardt *et al*., 2004a) has being used to analyse palaeointensity determinations of slab.I. Palaeointensities are generally defined on a sufficient number of points (N≥5) and a sufficient fraction of the NRM (generally 40%<f<60%; dotted-dashed curve in Fig.6.$_A$). The δ(t*) parameter is considered to be indicative of the grain size, and thus, of the domain state (Leonhardt *et al*., 2004b). The parameter decreases rapidly from high values (>20) at the base of the profile to low values, generally below 5 in most of the profile (black curve in Fig.6.$_A$). Values of δ(t*) exceeding 5 are thought to represent large PSD to MD grains, while δ(t*)-values inferior to 5 are believed to indicate small PSD to SD grains (Leonhardt *et al*, 2004b). Such reasoning tallies with the ore microscopy observation that lamellae were absent in samples from the lowermost part of the flow, and point to effectively larger grain sizes there.

Deviations of alteration checks indicate low alteration in the lower zone, but reach higher values in the upper zone. Check differences indicative of laboratory alteration, however, remain below 8% for all determinations. Even the cumulative alteration contribution is small, emphasised by the fact that the alteration correction method after Valet *et al*. (1996) does not fundamentally modify the overall palaeointensity results (Fig.6.$_A$), with an uncorrected value of 1.66 ±0.40 μT compared to 1.94 ±0.50 μT after correction (discarding data from the 4 first cm).

The zone dominated by small vesicles (lower zone) shows the smallest degree of laboratory alteration, which suggests that alteration already happened through geological times. Except for samples from the oxidised bottom zone, all palaeointensity determinations yield consistent results throughout slab.I.

4.3. Palaeodirections from slab.II

ACCEPTED MANUSCRIPT

The thermal demagnetisation of samples from slab.II seems to show merely the presence of two components (Fig.4.$_B$): a low temperature component C_{LT} defined from 80-120° to 360°C (after removal of minor viscous magnetisation) and a high temperature component C_{HT} from 480° to 560°C, when a viscous magnetisation is acquired (from 560° to 600°C). However, several indications suggest the existence of a third, mid-temperature component C_{midT}.

First of all, it would be surprising to observe three components in slab.I but only two components in slab.II, a block taken only at approximately 3 metres away from the first in the same lava flow. Moreover, the detailed analysis of the directions of magnetisation reveals a deviation of these directions in the mid temperature range, better visible using stereographic and 3D projections. On a stereographic projection, component C_{HT} forms an end-point (Fig.5.$_B$). The low temperature component C_{LT} is more or less well developed (see for instance specimen II-A-41 compared to II-C-35; Fig.5.$_A$), but some specimen show C_{LT} running directly to the end-point (LT_1 on the stereographic projection of Fig.5.$_B$) while others show C_{LT} running to another position (LT_2 in Fig.5.$_B$). Between this intermediate position and the end-point, corresponding to temperatures ranging from 360° to 480°C, must exist a mid temperature component C_{midT}. Although tenuous, the mid temperature component seems to be sufficiently well isolated in 13 specimens, the other samples showing an intermediate direction of magnetisation between C_{LT}, C_{midT} and C_{HT} in that temperature range (Fig.5.$_C$).

The definition of C_{LT} is often difficult because of the viscous magnetisation at low temperature and the overlap of unblocking temperature spectra with either C_{midT} or directly C_{HT}. The obtained directions of magnetisation are therefore scattered (Fig.5.$_C$ in core coordinates), but the overall mean direction is D:022.3° / I:13.6° (α_{95}=5.8°; κ=8.51; N=79, in stratigraphic coordinates). In the mid temperature range, the directions of magnetisation have generally no real meaning because they cannot be sufficiently well isolated, except presumably for 13 samples (5 in profile A and 8 in profile C) for which the mean direction is D:049.0° / I:25.4° (α_{95}=5.1°; κ=67.06; N=13). The overall mean direction for C_{HT} defined from PCA is D:087.3° / I:-03.1° (α_{95}=3.5°; κ=21.47; N=82; the peak density is oriented: 084.6° / -13.1°).

ACCEPTED MANUSCRIPT

It is striking to see an elongation in data distribution of C_{HT}, moreover, precisely in the prolongation of the position of the mean direction for C_{midT} (better seen in core coordinates; Fig.5.$_C$). Consequently, it is believed that the presence of C_{midT}, although very tenuous, influences the orientations of C_{HT}. It suggests that component C_{HT} is not properly isolated, although C_{HT} is defined from clear, linear segments covering more than 50% of the NRM and encompassing about 200°C of the thermal demagnetisation (Fig.4.$_B$ & 5.$_A$). In order to get rid of the influence of C_{midT} on C_{HT}, great circle analysis (McFadden, 1990) has been tested, although the superiority of this approach can be questioned given the limited extent of C_{midT} and the good linearity of C_{HT}. However, the overall mean direction obtained is D:092.6° / I:-07.4° (α_{95}=1.6°; κ=106.20; N=80).

The pole HT.$_{II}$ (Fig.7) corresponding to C_{HT} defined from linear segment (PCA) is: ϕ=076.90° / λ=01.70° (dp=1.73° / dm=3.46°), and falls close to the equator in the Indian Ocean. The pole midT.$_{II}$ (ϕ=081.61° / λ=42.19°; dp=2.96° / dm=5.49°) is situated at the boundary between Kazakhstan and China, and pole LT.$_{II}$ (ϕ=114.93° / λ=60.19°; dp=3.03° / dm=5.93°) is located in Siberia, at about 60° in latitude, north of the Baikal Lake.

Important discrepancies exist when the directions of magnetisation of component C_{HT} from profiles A and C are compared according to samples position in slab.II (Fig.6.$_B$). Large differences appear for samples situated where the change in vesicles size is delimited, and the most striking and obvious variations are attributed to samples positioned where the rock is broken.

4.4. Palaeointensities from slab.II

Palaeointensity determinations for the samples of slab.II are mostly of better quality compared to slab.I, however returning similar overall results. The fraction of the NRM used to define palaeointensities is large (generally 50%<f<80%; dotted-dashed curve in Fig.6.$_B$), and the number of points, considered sufficient (N≥5). The δ(t*) parameter is relatively constant throughout the profile

ACCEPTED MANUSCRIPT

(solid black curve in Fig.6.$_B$), with values generally below 5 indicating the presence of small PSD to SD grains, except for samples corresponding to fractures or cracks in the rock.

Alteration is revealed by slightly higher values of the δ(CK) parameter (solid grey curve in Fig.6.$_B$) in the lower zone [5-18 cm] than in most of the upper zone [21-32 cm], with a decrease approximately coincident with the change in vesicles size. Like for slab.I, the laboratory alteration is (except for the cracks) always below 9%, and the cumulative alteration is insignificant. The mean palaeointensity value is 2.62 ±1.02 µT (and 2.70 ±1.09 µT if the cumulative alteration effects are corrected), when data from the 5 first centimetres and at 34 cm and 45 cm are discarded (Fig.6.$_B$).

5. Discussion

5.1. Directional component

Three components, C_{HT}, C_{midT} and C_{LT}, have been determined in the two slabs. They are all interpreted to be associated with the "El Paso" Earth magnetic reversal, because their corresponding VGPs are located between the Equator and 60° in latitude (Fig.7). The origin of the different components and their time of acquisition, however, are subject to discussion.

The emplacement of the lava flow is thought to be accompanied by high temperature deuteric oxidation giving rise to the exsolution of ilmenite lamellae, which led to the division of rather large grains (~8 µm, based on ore microscopy imagery analysis) of titano-magnetite into small PSD to SD particles of titanium-poor (~7-8%) titano-magnetite. These small particles carry the stable component C_{HT} and recorded the Earth's magnetic field during cooling of the flow. In other words, these small particles acquired a TRM witnessing a VGP position close to the Equator, south of India, and a very weak field intensity in the order of 2 µT, *i.e.* about 20 times weaker than the present-day field in Gran Canaria (~38.4 µT).

The directions of magnetisation corresponding to C_{HT}, however, show the strongest deviations close to fractures and cracks, but are also influenced by the presence of vesicles, particularly visible where changes in vesicles size occur. It results in an elongation of the distribution of directions of

ACCEPTED MANUSCRIPT

magnetisation. In slab.II, this elongation is readily linked to component C_{midT}. When great circles analysis is used to get rid of the influence of C_{midT} on C_{HT} in slab.II, the overall mean direction is remarkably consistent with the intersection of the two great circles best fitting the elongation of the two distributions of components C_{HT} for slab.I and slab.II (D:092.6° / I:-07.4° for $C_{HT\text{-}II}$ from great circles analysis, and D:092.0° / I:-06.0° for the intersection of the two great circles fitting $C_{HT\text{-}I}$ and $C_{HT\text{-}II}$; see corresponding VGPs in Fig.7).

The ring of alteration around the vesicles suggests that the volatiles (*e.g.* probably H_2O, CO_2) contained inside the bubbles diffused in the surrounding matrix. In the lower zone, oxidised areas are more widespread, presumably because vesicles are smaller but more numerous, increasing the surface of contact between volatiles and matrix. In the upper zone, vesicles are larger and rings of alteration are usually better delimited. It is believed that gas diffusion caused low temperature oxidation of magnetic minerals, explaining variations in magnetic properties along the profiles, and in particular, the presence of (titano-)maghaemite revealed by thermomagnetic curves in low (14 mT) field.

The variation of component C_{HT} in association with vesicles size and the influence of component C_{midT} on C_{HT} suggest that C_{midT} is of (thermo-)chemical origin. The diffusion of volatiles from the vesicles into the nearby matrix may have altered at different degrees the magnetic carrier of C_{HT} (Ti-magnetite) into a new type of material (Ti-maghaemite), which acquired a (thermo-)chemical remanent magnetisation ((T)CRM). The position of the pole $midT_{.II}$ (Fig.7) supposes, however, a different orientation of the Earth's magnetic field during the acquisition of this (T)CRM. Note, moreover, that it is only possible to distinguish between the primary magnetisation (C_{HT}) and the overprint (C_{midT}) probably because the field was in an intermediate state and changes in orientations are sufficiently large.

Unfortunately, it is not possible to determine the time of acquisition of C_{midT} relative to C_{HT}, and therefore, whether the changes of Earth's magnetic field state occurred rapidly or not. The diffusion of volatiles into the matrix could be part of the lava flow cooling, and could correspond to the final stage of the degassing at low temperature. This hypothesis entails that the Earth's magnetic field might have changed quite rapidly depending on the diffusion rate, because the pole $midT_{.II}$ is clearly distinct from

ACCEPTED MANUSCRIPT

pole $HT._{II}$ (Fig.7). On the other hand, porosity and permeability measurements cannot rule out that a fluid (or gas) might have percolated later through the lava flow, in particular through the vesicles. In this case, alteration triggered by the infill of the vesicles would be thus a later event, accounting for the large distance between pole $midT._{II}$ and pole $HT._{II}$.

Component C_{LT} is clearly different from the orientation of the present-day field. The pole LT_{II}, at 60° in latitude, is also distinct from a stable dipolar position of the Earth's magnetic field. The acquisition of C_{LT}, therefore, is interpreted to be still related to the recording of the Earth magnetic reversal.

Yet, the origin of C_{LT} cannot be determined. It is likely that component C_{LT} is associated to later hydrothermal alteration. However, given the temperature range for the determination of C_{LT} (80° – 240°C), it can be related either to chemical changes of magnetic minerals in contact with a percolating fluid (acquisition of a CRM), or to the acquisition of a thermal (or thermo-chemical) magnetisation caused by the elevation of the ground temperature due to hot fluid (TRM or TCRM).

To sum up, component C_{HT} is interpreted to be a TRM of primary origin. The origin of components C_{midT} and C_{LT} may have predominantly two causes:

1 – C_{midT} and C_{LT} correspond to two phases of hydrothermal alteration, *i.e.* two pulses of fluid percolation into the vesicles and acquisition of (T)CRMs.

2 – If the rock is regarded as impermeable where cracks and failures are absent, C_{midT} can correspond to a CRM related to the final stage of the lava flow degassing, *i.e.* the "primary" volatiles diffused in the matrix and altered (oxidised) the magnetic carrier of C_{HT}. A later circulation of hot fluid in cracks and around the lava flow increased the ground temperature and provoke the acquisition of a TRM (or TCRM) corresponding to C_{LT}.

5.2. Diurnal field variations recorded?

After the directional analysis presented above, which followed a more traditional palaeomagnetic recipe, we now analyse the thermal demagnetisation according to scheme of the companion paper

ACCEPTED MANUSCRIPT

(Winklhofer *et al.*, *this issue*). For this purpose, the direction recovered after each thermal demagnetisation step is plotted in function of vertical position within the flow. Such representation of the directional data allows one, in principle, to identify an external field variation recorded in the flow by the characteristic pattern it imprints on the thermoremanence distribution, with two diagnostic properties: 1) the variations have larger amplitudes at higher unblocking temperature, since cooling rates are faster at higher temperature, which in turn results in a better temporal resolution and causes less smoothing; and 2) variations are shifted in position away from the interior of the flow with lower unblocking temperatures, because time dependent signals are blocked along cooling isochrons, which run at oblique angles through the flow.

When looking at the diagrams (Fig.8), the amplitudes of the directional variations generally seem to increase with decreasing blocking temperature, a trend which is opposite to what is expected for a recorded external field variation. Moreover, the directional orientations vary in a rather unsystematic fashion with depth and are quite large. The variations rather are fixed to discrete depth points. The observation of stationary signals is at odds with the second characteristic property of an external variation, requiring a shift of the signal with depth coordinate. We therefore interpret those variations that are fixed to discrete depth points as an overprint signature (see below, section 5.3).

Nonetheless, in some portions of the profiles where there is less overprint, one can notice some subtle phase shifts in amplitude that appear to be in agreement with the theoretical predictions for an external variation. For example, the declination patterns of profile C in slab.I (Fig. 8a), near the top (30 cm) and the bottom (10 cm) of the flow show a subtle shift in position away from the central part as the unblocking temperature decreases from 515°C to 450°C. Judging from the raggedness of the variations, this may be just coincidence - even more so because shifts in position toward the central part of the flown can be seen as well. The overprint also limits the possibility of tracking further phase shifts through the demagnetization diagrams. We are therefore not in a position to identify a trapped external field variation unambiguously.

5.3. Magnetic overprint

ACCEPTED MANUSCRIPT

The stable (high-temperature) end-point was determined as D:92° / I:-06° using great circles intersection. Next, we ask how the remanence, say at 500°C, is affected by overprint in function of profile coordinates. A simple measure for this purpose is the angular deviation of the actual remanence vector at 500°C from the stable end-point vector. The results are summarised in Fig.9.$_A$ (slab.I) and 9.$_B$ (slab.II). It can be seen that the angular deviation varies substantially and in a non-systematic manner with depth. The number of samples affected by moderate overprint (20°-30°) is larger in slab.I (Fig.9.$_A$) than in slab.II (Fig.9.$_B$). Also, the two adjacent profiles A and C (spacing 2 cm) of slab.I appear to be affected by overprint in a more coherent way than the profiles A and C from slab.II of the same flow. The influence of overprint on slab.I is stronger in the basal part (reddish colour, higher Curie-temperature), while slab.II shows strong overprint also in the more central part, which is linked to individual points in the flow rather than being penetrative.

On the basis of ore microscopy, the overprint was attributed to the growth of secondary minerals. Rock magnetic parameters should indicate the presence of overprint, provided that the overprint-bearing phases are different from the phases that carry the primary remanence, or at least, have largely different magnetic grain sizes. In the profiles presented, one can see a systematic trend in the depth-dependence of the rock magnetic parameters, which seems to have been imprinted already by the cooling history. Superimposed on the systematic trend in some rock magnetic parameters (M_S, susceptibility) are short-scale perturbations, which roughly coincide with those positions in the flow that are noticeably affected by overprint. The correlation can only be roughly established, since hysteresis and isothermal remanence parameters were not measured directly on the same samples used for direction analysis (thermal demagnetisation up to 600°C), but on sister samples. Due to the localised nature of the overprint and the small sample sizes used, it is likely that sister samples are not always representative to each other, which limits the robustness and statistical significance of the correlation procedure. Of all parameters measured, M_{RS}, M_S and susceptibility (mass-normalised) are the only ones that, through lowered values, (roughly) indicate overprint, which points to overall less

ACCEPTED MANUSCRIPT

magnetic material in the overprinted samples (for example, due to leaching by the pore fluids), or the partial replacement of a more strongly magnetic primary phase by a more weakly magnetic phase.

6. Conclusions

The two investigated blocks are characterised by an isotropic magnetic fabric, a coherent thermal demagnetisation behaviour marked by consistent unblocking temperature spectra for almost all samples, very similar Curie temperatures (540°C), which indicates titanium-poor (~7-8%) titano-magnetite as main magnetic carrier, and a homogeneous grain size distribution dominated by SD/PSD behaviour. In detail, however, there are important variations in magnetic properties along the vertical axis, but also along the horizontal axis. Significant variations are observed particularly in relation to fractures and vesicle sizes, affecting the degree of alteration. Therefore, even in thin lava flow profiles, important variations in magnetic properties affect the determination of palaeodirections and palaeointensities emphasizing the need for carefully selecting the least altered parts in standard palaeomagnetic sampling. For the specific lava flow studied here, the overall palaeopole (taken as the intersection of the two great circles; see Fig.7) is located on the Equator (ϕ=075.95° / λ=-03.19°), south of India, and the overall mean palaeointensity value is 2.32 ±1.40 µT (after alteration correction). These results are in good agreement with the values reported by Leonhardt & Soffel (2002) and Leonhardt *et al*. (2002), and confirm the drop in the Earth's magnetic field intensity during a reversal.

Nevertheless, the magnetisation directions vary considerably during thermal demagnetisation with depth coordinate in the flow. Directional variations between different directional magnetisation components suggest that magnetic overprints occurred relatively soon after emplacement. Most of the directional variations are attributed to secondary minerals, formed by fluid diffusion related to presence of vesicles. Dramatic variations are found to be associated with fractures or cracks in the rock. A characteristic rock magnetic manifestation of these overprints, however, is only found in concentration related parameters like M_S, M_{RS} and susceptibility.

ACCEPTED MANUSCRIPT

Secondary magnetisations significantly hamper the recognition of possible characteristic directional variations in amplitude and phase shift, which would allow for an unambiguous identification of external diurnal geomagnetic field variations. Although subtle, phase shifts are apparent in some regions of the demagnetisation diagrams, which are least affected by overprint, and indeed appear to be consistent with the theoretical predictions of (Winklhofer *et al*., *this issue*). However, the overprint in adjacent regions makes it impossible to further constrain the nature of the phase shift. The question therefore has to remain open as to whether or not the fragmentary phase shift is a fingerprint of diurnal external variations.

Acknowledgments:

This work was funded by Deutsche Forschungsgemeinschaft (DFG project Wi 1828/3-1). We are grateful to three different anonymous reviewers for their helpful comments.

References

Ade-Hall, J.M., Palmer, H.C., and Hubbard, T.P., 1971. The magnetic and opaque petrological response of basalts to regional hydrothermal alteration. Geophysical Journal of Royal Astronomical Society, 24: 137-174.

Cande, S.C., and Kent, D.V., 1995. Revised calibration of the geomagnetic polarity timescale for the Late Cretaceous and Cenozoic. Journal of Geophysical Research, 100: 6093-6095.

Day, R., Fuller, M., and Schmidt V.A., 1977., Hysteresis properties of titano-magnetites: grain-size and compositional dependence. Physics of Earth and Planetary Interiors, 13: 260-267.

Jelínek, V., 1981. Characterization of the magnetic fabric of rocks. Tectonophysics, 79: 63-70.

Kirschvink, J.L., 1980. The least-squares line and plane and the analysis of palaeomagnetic data. Geophysical Journal of the Royal Society, 62: 699-718.

Krása, D., Heunemann, C., Leonhardt, R. and Petersen, N., 2003. Experimental procedure to detect multidomain remanence during Thellier-Thellier experiments. Physics and Chemistry of the Earth, 28: 681-687.

Leonhardt, R., 2006. Analyzing rock magnetic measurements: The RockMagAnalyser 1.0 software. Computers and Geosciences, 32 (9): 1420-1431.

Leonhardt, R., and Soffel, H.-C., 2002. A reversal of the Earth's magnetic field recorded in mid Miocene lava flows of Gran Canaria, Paleointensities. Journal of Geophysical. Research, 107: 2299, doi:10.1029/2001JB000949.

Leonhardt, R., Heunemann, C., and Krása, D., 2004a. Analyzing absolute paleointensity determinations: Acceptance criteria and the software Thellier Tool 4.0. Geochemistry, Geophysics, Geosystems (G^3), 6 (1): 11 pp.

Leonhardt, R., Krása, D., and Coe, R.S., 2004b. Multidomain behavior during Thellier experiments: A phenomenological model. Physics of Earth and Planetary Interior, 147: 127-140.

ACCEPTED MANUSCRIPT

Leonhardt, R., Matzka, J., and Menor, E.A., 2003. Absolute paleointensities and paleodirections from Fernando de Noronha, Brazil. Physics of Earth and Planetary Interiors, 139: 285-303

Leonhardt, R., Matzka, J., Hufenbecher, F., Heider, F., and Soffel, H.-C., 2002. A reversal of the Earth's magnetic field recorded in mid Miocene lava flows of Gran Canaria, Paleodirections. Journal of Geophysical. Research, 107: 2024, doi:10.1029/2001JB000322.

McFadden, P., 1990. A new fold test for paleomagnetic studies. Geophysical Journal International, 103: 163-169.

Moskowitz, B.M., 1981. Methods for estimating Curie temperatures of titanomagnetites from experimental J_s-T data. Earth and Planetary Science Letters, 53: 84-88

Müller, S., Melnik, O., Spieler, O., Scheu, B., and Dingwell, D.B., 2005. Permeability and degassing of dome lavas undergoing rapid decompression : an experimental decompression. Bulletin of Volcanology, 67 (6): 526-538.

Riisager, P., and Riisager, J., 2001. Detecting multidomain magnetic grains in Thellier paleointensity experiments. Physics of Earth and Planetary Interior, 125: 111-117.

Saito, T., Sakurai, T., and Yumoto, K., 1978. The Earth's palaeomagnetosphere as the third type of planetary magnetosphere. Planetary and Space Science, 26 (5): 413-422.

Siscoe, G.L., and Crooker, N.U., 1976. Auroral zones in a quadrupolar magnetosphere, Journal of Geomagnetism and Geoelectricity, 28: 1-9.

Tauxe, L., 1998. Paleomagnetic principles and practice. Modern approaches in geophysics, 17, Monograph title, Kluwer Academic Publishers, Dordrecht, Netherlands, 299 pp.

Ultré-Guérard, P., and Achache, J., 1995. Core flow instabilities and geomagnetic storms during reversals: The Steens Mountains impulsive field variations revisited. Earth and Planetary Science Letters, 135: 91-99.

Valet, J.-P., Brassart, J., Le Meur, I., Soler, V., Quidelleur, X., Tric, E., and Guillot, P.-Y., 1996. Absolute paleointensity and magnetomineralogical changes. Journal of Geophysical Research, 101: 25029-25044.

Winklhofer, M., Fabian, K., Leonhardt, R., and Vérard, C., 2008. On the possibility of recovering paleo-diurnal magnetic variations in transitional lava flows: 1) Constraints from thermoremanence modelling for an experimental protocol. *This issue*.

Zieger, B., Vogt, J., Glassmeier, K.H., Gombosi, T.I., 2004. Magnetohydrodynamic simulation of an equatorial dipolar paleomagnetosphere. Journal of Geophysical. Research, 109: A07205.

Accepted Manuscript

ACCEPTED MANUSCRIPT

Figure captions

Figure 1 – Morphology and magnetic properties of slab.I & slab.II cut out block.I & block.II oriented in the field . The shape of the slabs, where cores were drilled every centimetre, is shown in the middle with its zones (see text). The graphs, showing the measured values according to the position in centimetres in the slab, are from ***left to right***: the absolute volume (black line) and mass (grey line) susceptibility; the coercivity (B_C; grey line) and coercivity at remanence (B_{CR}; black line); the saturation magnetisation (M_S; grey line) and saturation magnetisation at remanence (M_{RS}; black line); and the Curie point (T_C).

A: Magnetic properties for slab.I; **B**: For slab.II.

Figure 2 – A: Example of hysteresis and thermomagnetic curves for three samples, taken at 3, 15 and 30 cm from the base of slab.I. ***Above***: Thermomagnetic curves in "high" field (169 mT), and used to determine Curie points; ***below***: Thermomagnetic curves in "low" field (14 mT). Note the increase in magnetisation at around 200°C corresponding to the inversion of (titano-)maghaemite. **B:** Photographs of two polished sections from slab.I examined in oil using reflected light microscopy. ***Left***: Polarised light, and ***right***: polarised and analysed light. Some grains show both high temperature deuteric oxidation (see exsolution of ilmenite lamellae in enlarged grain) and low temperature oxidation (highlighted by a reddish colour in polarised and analysed light). In the upper zone (19-22 cm), the matrix is relatively preserved from oxidation (black magnetic grains in polarised-analysed light), and alteration is predominantly concentrated in rings around vesicles (white mass at the bottom right).

Figure 3 – Unblocking temperature surface (or "unblocking spectra map") corresponding to the first derivative (slope) of all thermal demagnetisation curve placed next to one another according to the position of samples in slab.I (for profiles A, B and C). Note the variations for the five first centimetres and where the rock is broken.

Accepted Manuscript

ACCEPTED MANUSCRIPT

Figure 4 – Examples of palaeodirection and palaeointensity results. From ***left to right***: Orthogonal projection with open (close) symbols corresponding to the projection on vertical [V] (horizontal [H]) plane; Stereographic "Schmidt" equal area projection (Stars correspond to the NRM at room temperature; data points are shown in grey when the signal becomes unstable); Demagnetisation curve (solid black circles; grey boxes correspond to the first derivative) and susceptibility (open grey circles, measured with a minikappa KLF-3) normalised to one; Arai diagram (white circles: thermal demagnetisation; white triangles: pTRM* checks; grey squares: repeated demagnetisation steps; grey segment: fraction used to calculate the palaeo-intensity).

A: For slab.I; **B**: For slab.II.

Figure 5 – Problem of proper identification of components C_{LT} and C_{midT} in slab.II. **A:** Examples of orthogonal projection where C_{LT} is just too weak (specimen (II-C-35), or overlapped with a viscous component (Visc.; specimen II-A-41), and where component C_{midT} is not really obvious (specimen II-A-01 and II-C-34). **B:** Component C_{midT}, however, can be defined in some cases using stereographic projection (or with 3D orthogonal projection). For example, the low temperature component (LT_1) directly overlaps the high temperature component (HT) for specimen II-A-01, but the low temperature component for specimen II-C-34 (LT_2) is "displaced" by a mid-temperature component. **C**: Directions of magnetisation for slab.II shown in stereographic projection, in core coordinates; open symbols: upper hemisphere, closed symbols: lower hemisphere. Note that the overall mean direction for all single directions in mid temperature range correspond to a mixture between C_{LT}, C_{midT} and C_{HT}, since it falls inside a triangle (dashed line) defined by these three components; note also that the distribution of the high temperature data points is elongated on the edge of this triangle, between C_{midT} and C_{HT}.

Figure 6 – Palaeodirection and palaeointensity determinations of each slab (shape shown in the middle). The graphs, showing the measured values according to the position (in cm from base) in the slab, are from ***left to right***: the palaeodeclination (black squares for samples from profile A, and grey circles, from profile C, shown with their maximum angular deviation (MAD) in degrees (°); the palaeoinclination (squares for samples from profile A, and circles, from profile C, shown with their

ACCEPTED MANUSCRIPT

MAD; dark grey line and light grey zone correspond to the overall mean declination & inclination and associated α_{95} respectively in degrees (°); the palaeointensity in micro-Tesla (μT) before alteration correction (black line) and after alteration correction (grey line) and their corresponding reliability classes (A, B & C before correction, and A*, B* & C* after correction); parameters associated with palaeointensity determinations (f: fraction of the NRM (×10, *i.e.* given between 0 and 10) used for the calculation; CK-error: % difference with checks; δ(t*): used as grain size indication (<5, SD behaviour; >5, MD behaviour), see Leonhardt *et al*. (2004a & 2004b).

A: Determinations for slab.I; **B**: For slab.II.

Figure 7 – Corresponding Virtual Geomagnetic Pole (VGP) positions. Orthogonal projection centred on 075°E/10°N; major grid spacing: 30°, minor grid spacing: 5°. Symbols are shown filled in white for slab.I and in grey for slab.II. Lozenge: pole LT corresponding to component C_{LT}; star: pole corresponding to all directions of the mid temperature range, and triangles: pole mid-T corresponding to C_{midT} (*i.e.* clusters 1 & 2 in slab.I and "well isolated" component in slab.II); circles: pole HT corresponding to C_{HT} (calculated from linear segment (PCA) and great circle analysis concerning slab.II); great circles (with dots marked every 5°) best fitting the elongation of the distribution of HT poles are shown in black (slab.I) and in grey (slab.II).

Figure 8: Single specimen directional data plotted against depth coordinate for each thermal demagnetization step. D´ [deg] is the variation of the declination relative to the mean value for that given unblocking temperature. The scale bar is the same for all graphs in each diagram. Note that the variations are, by and large, fixed in position, that is, they are independent of unblocking temperature, which reflects localised overprint (for example, associated with cracks or filled vesicles). (a) Diagram for profile C of slab I, (b) for profile A of slab I. Regions in the diagram with strong overprint are deleted (e.g, in the central part of a).

Figure 9: Angular deviation from single specimen palaeodirections (recovered at 500°C) from the direction of intersection between the two great circles for slabs.I & II. The intersection vector is

ACCEPTED MANUSCRIPT

oriented 092.02°/-06.00°. The angular deviation is a measure of how much the high temperature component is affected by overprint.

Accepted Manuscript

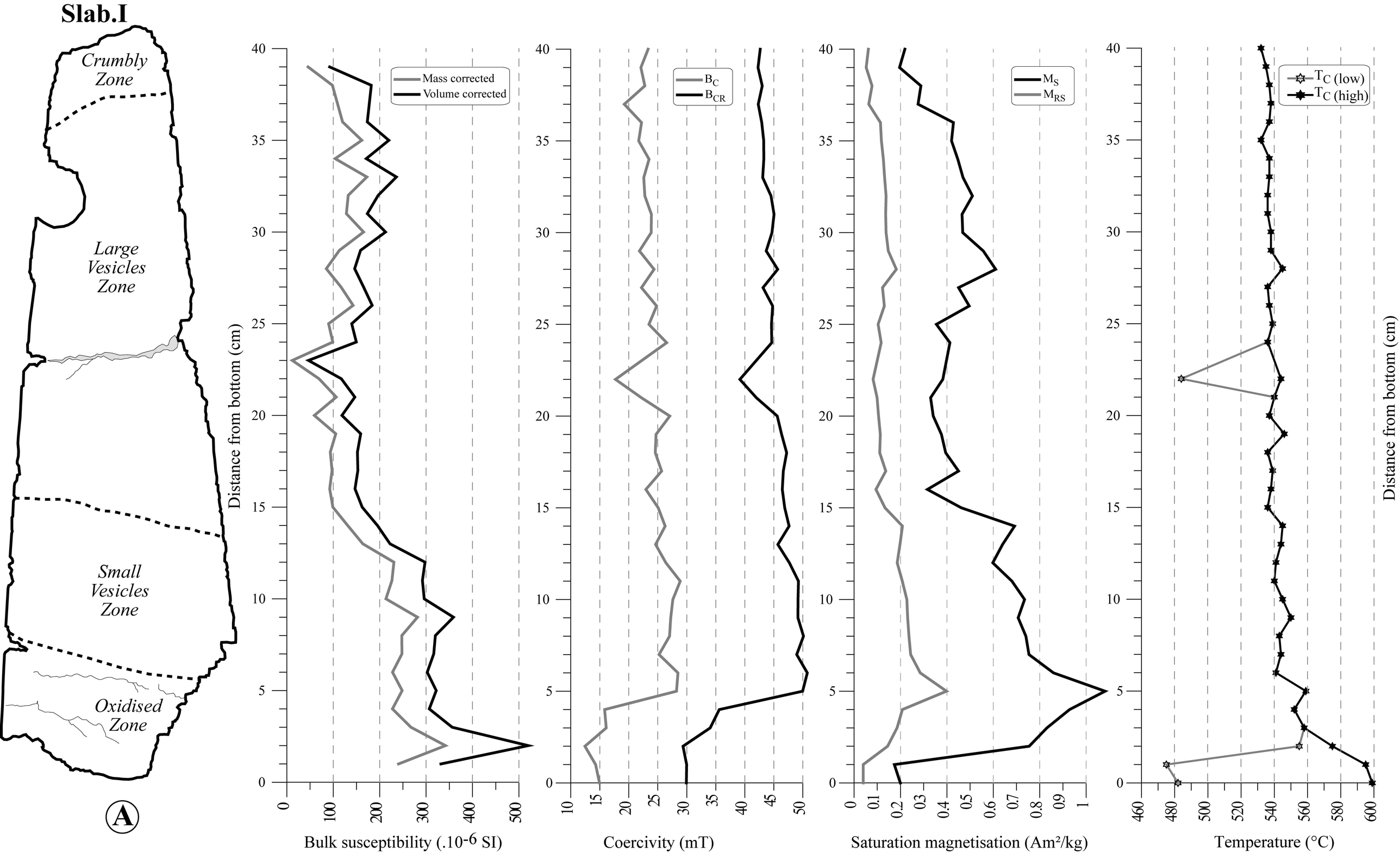
Slab.I
Crumbly Zone
Large Vesicles Zone
Small Vesicles Zone
Oxidised Zone
A
Distance from bottom (cm)
Mass corrected
Volume corrected
Bulk susceptibility (.10-6 SI)
BC
BCR
Coercivity (mT)
MS
MRS
Saturation magnetisation (Am²/kg)
TC (low)
TC (high)
Temperature (°C)

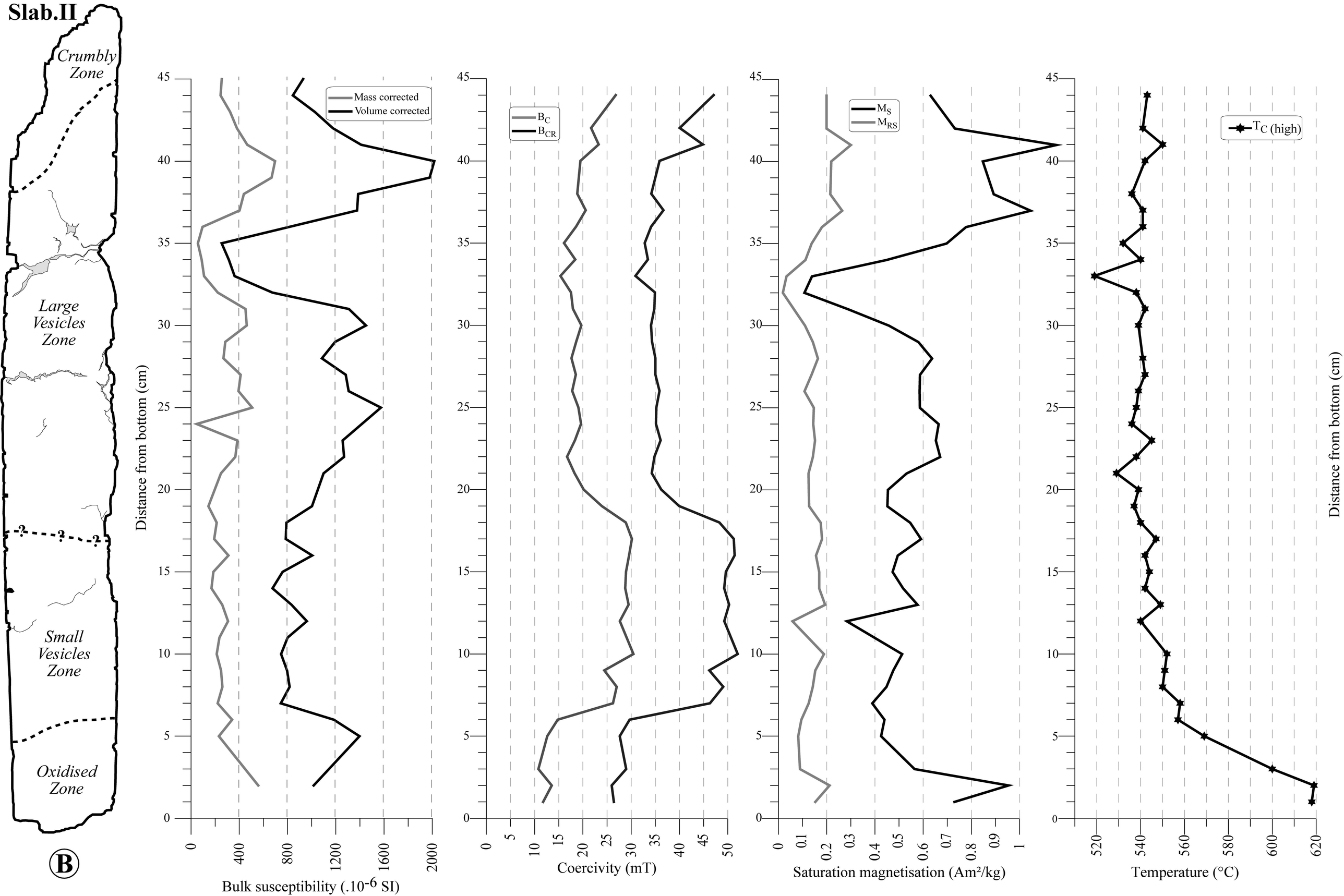
Slab.II
Crumbly Zone
Large Vesicles Zone
Small Vesicles Zone
Oxidised Zone
B
Distance from bottom (cm)
Mass corrected
Volume corrected
Bulk susceptibility (.10-6 SI)
BC
BCR
Coercivity (mT)
MS
MRS
Saturation magnetisation (Am²/kg)
TC (high)
Temperature (°C)

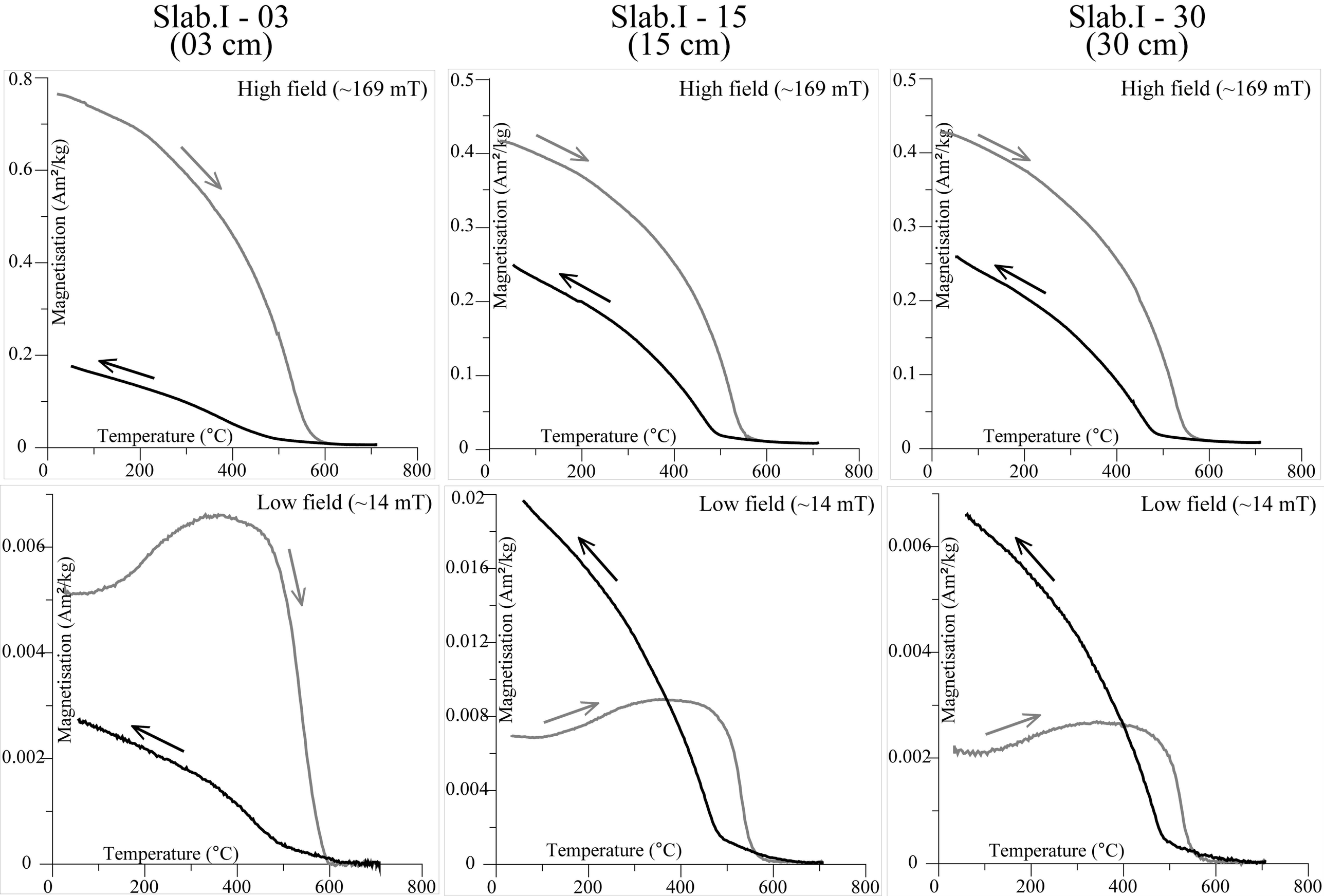
Slab.I - 03
(03 cm)
Slab.I - 15
(15 cm)
Slab.I - 30
(30 cm)
High field (~169 mT)
Low field (~14 mT)
Magnetisation (Am²/kg)
Temperature (°C)
0
200
400
600
800
0.8
0.6
0.4
0.2
0.5
0.3
0.1
0.02
0.016
0.012
0.008
0.006
0.004
0.002

Slab.I, between ~11 and 14 cm (from the bottom)

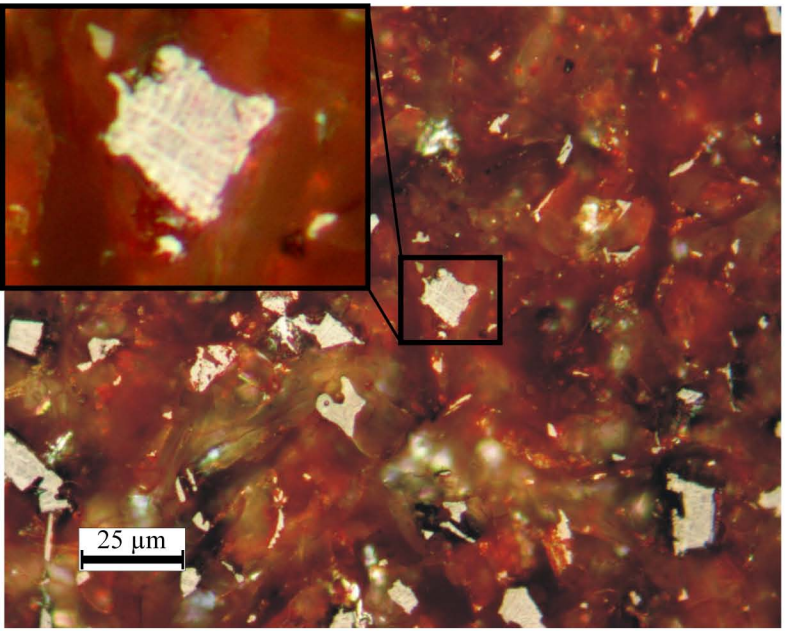

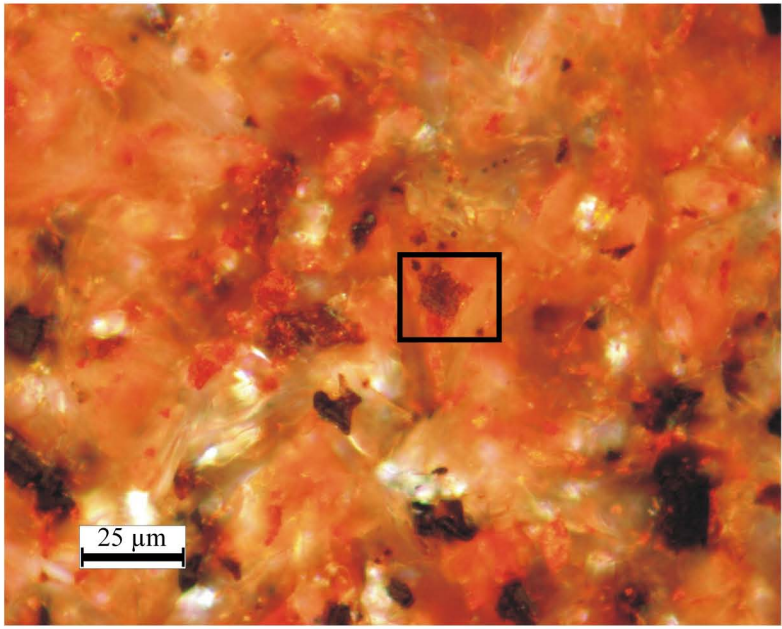

Slab.I, between ~19 and 22 cm (from the bottom)

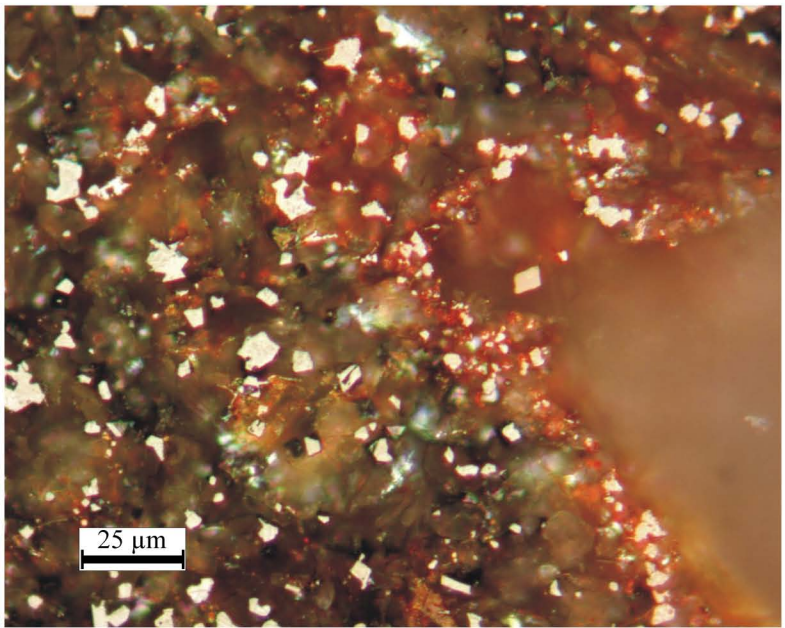

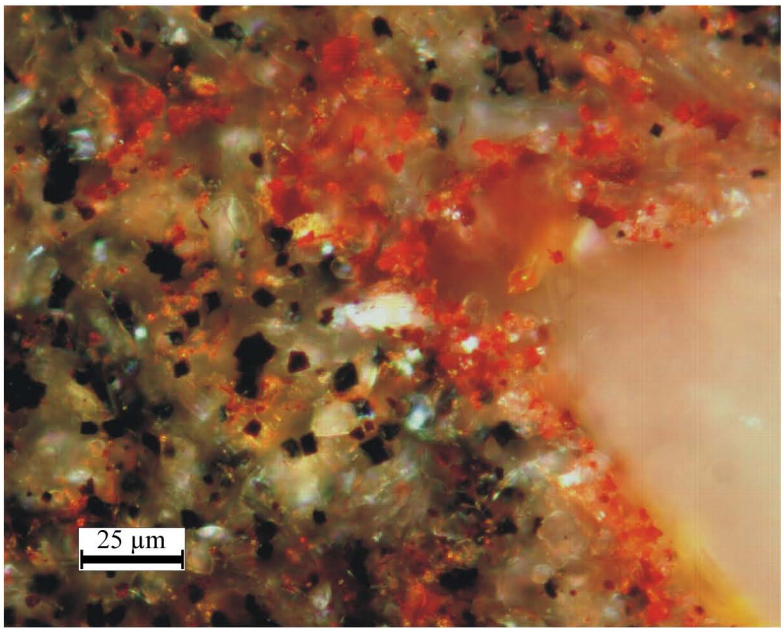

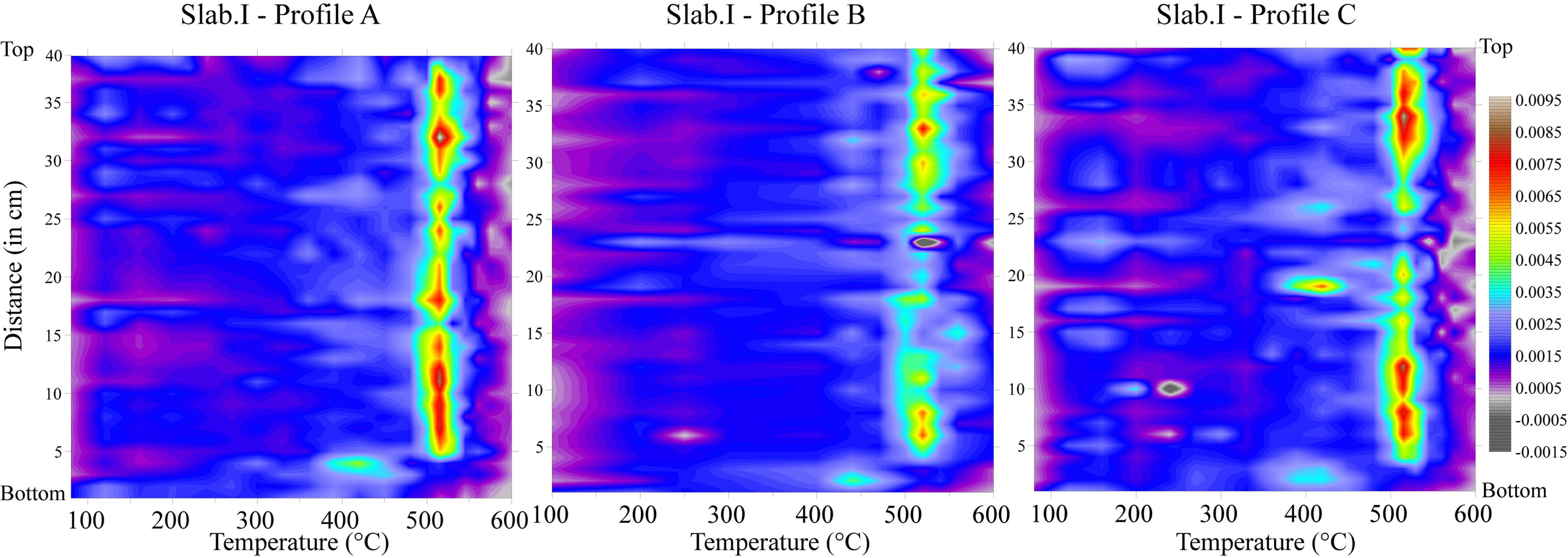
Slab.I - Profile A
Slab.I - Profile B
Slab.I - Profile C
Top
Bottom
Distance (in cm)
40
35
30
25
20
15
10
5
100
200
300
400
500
600
Temperature (°C)
0.0095
0.0085
0.0075
0.0065
0.0055
0.0045
0.0035
0.0025
0.0015
0.0005
-0.0005
-0.0015

Slab.I

A

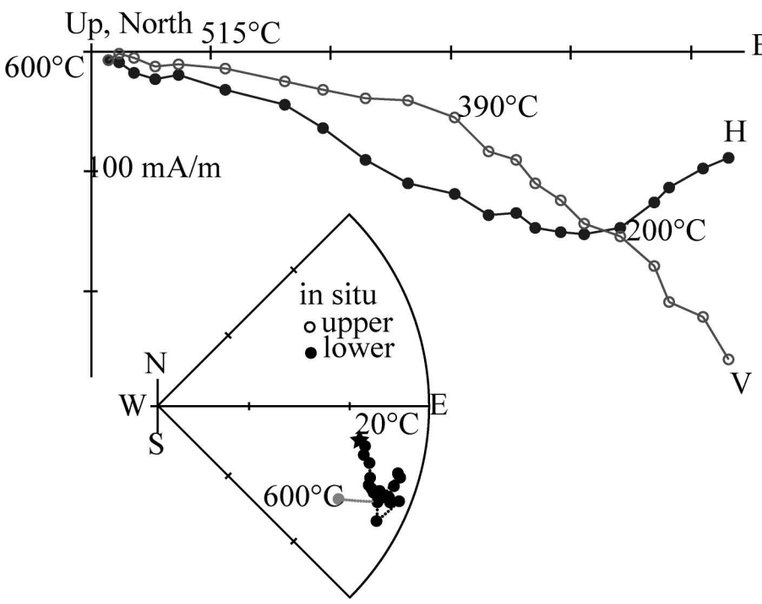
Up, North
515°C
600°C
East
390°C
H
100 mA/m
200°C
V
in situ
upper
lower
N
W
E
S
20°C
600°C

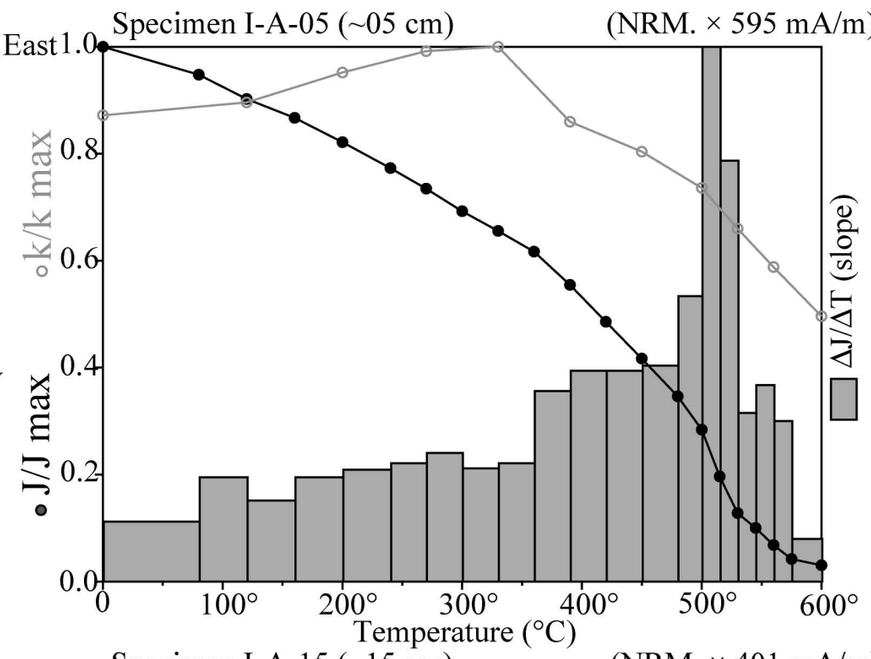
Specimen I-A-05 (~05 cm)
(NRM. × 595 mA/m)
k/k max
J/J max
ΔJ/ΔT (slope)
Temperature (°C)

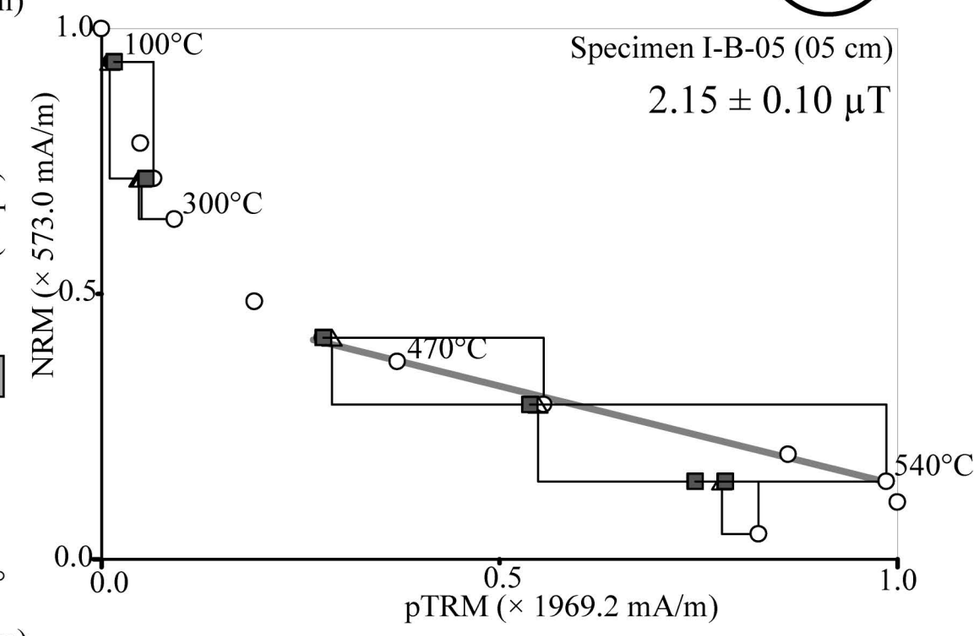
Specimen I-B-05 (05 cm)
2.15 ± 0.10 μT
100°C
300°C
470°C
540°C
NRM (× 573.0 mA/m)
pTRM (× 1969.2 mA/m)

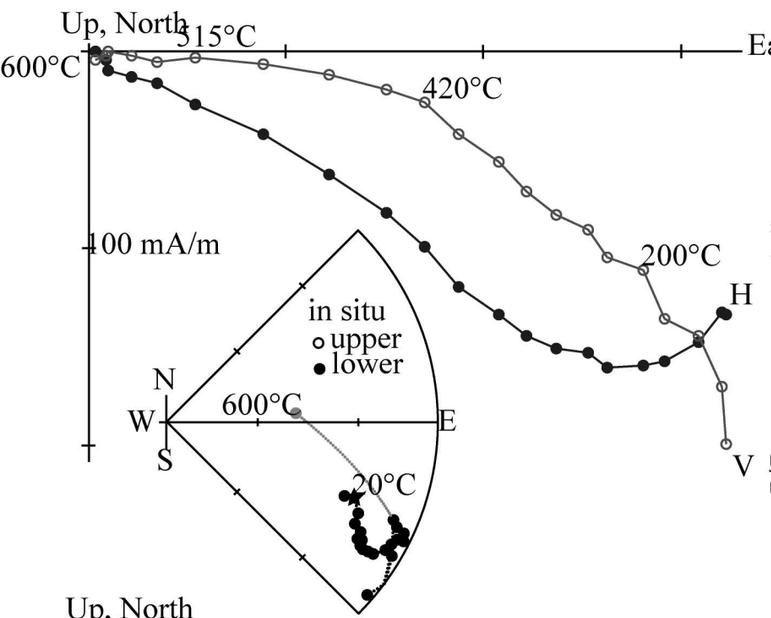
Up, North
515°C
600°C
East
420°C
100 mA/m
200°C
H
in situ
upper
lower
N
W
E
S
600°C
20°C
V

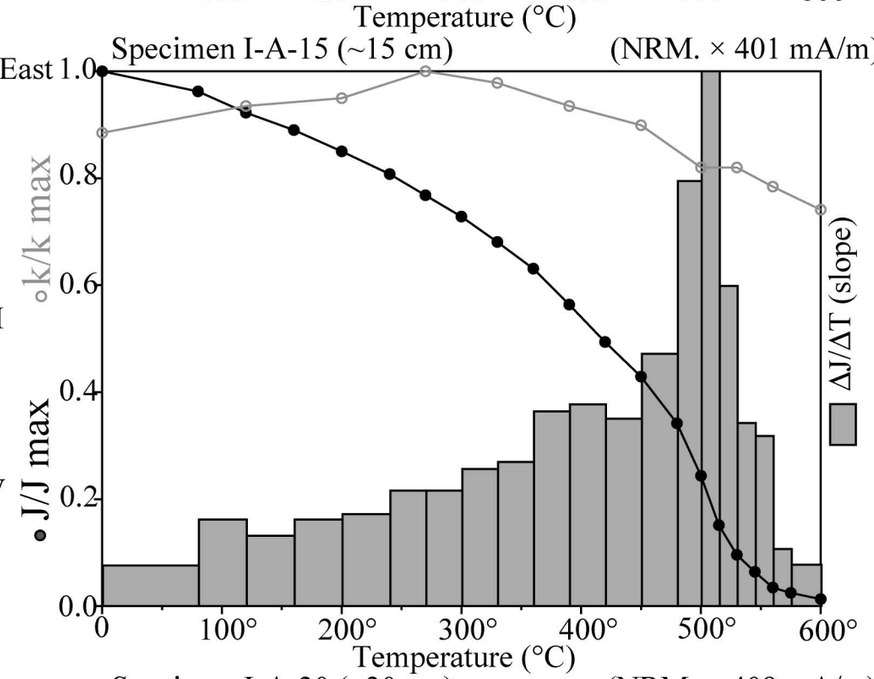
Specimen I-A-15 (~15 cm)
(NRM. × 401 mA/m)
k/k max
J/J max
ΔJ/ΔT (slope)
Temperature (°C)

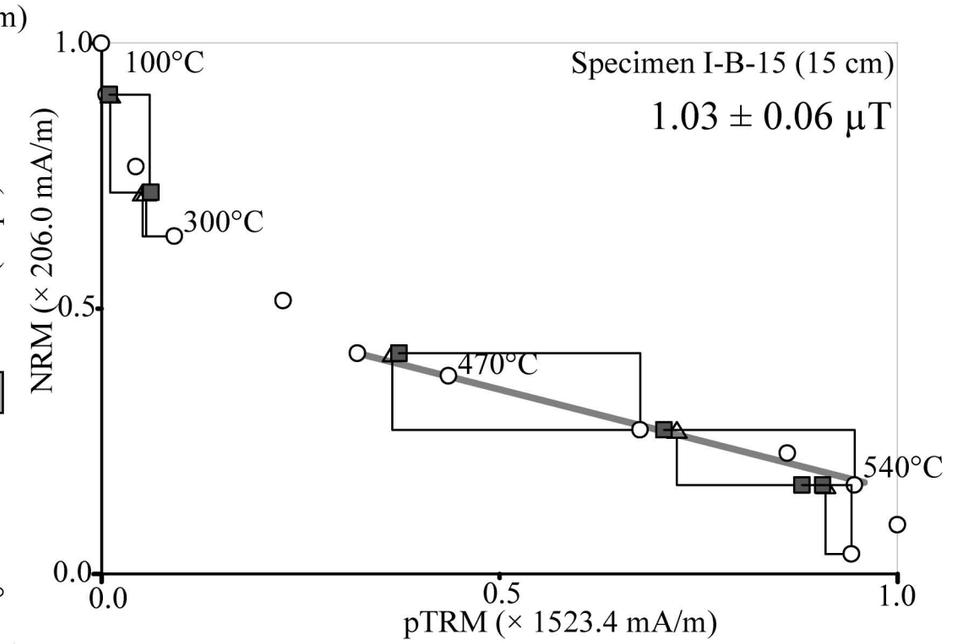
Specimen I-B-15 (15 cm)
1.03 ± 0.06 μT
100°C
300°C
470°C
540°C
NRM (× 206.0 mA/m)
pTRM (× 1523.4 mA/m)

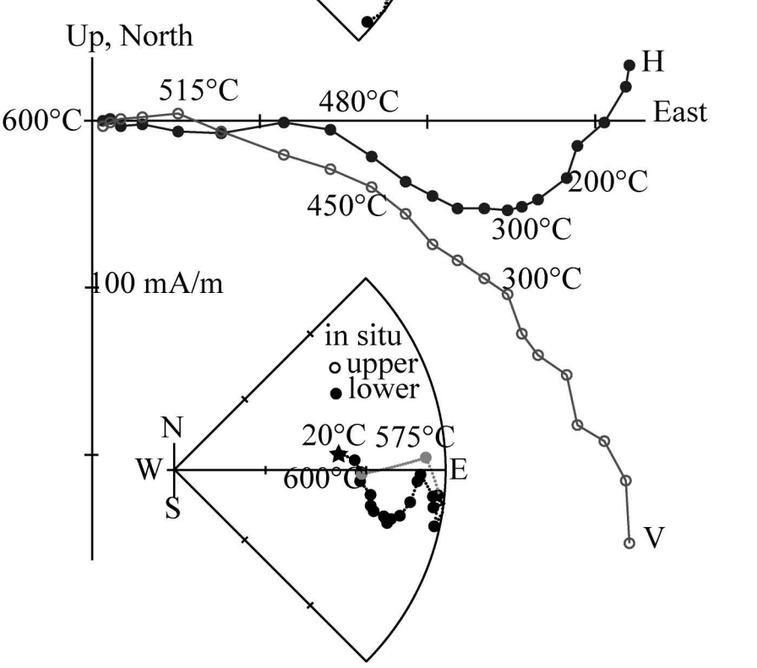
Up, North
H
515°C
480°C
East
600°C
200°C
450°C
300°C
300°C
100 mA/m
in situ
upper
lower
N
W
E
S
20°C
575°C
600°C
V

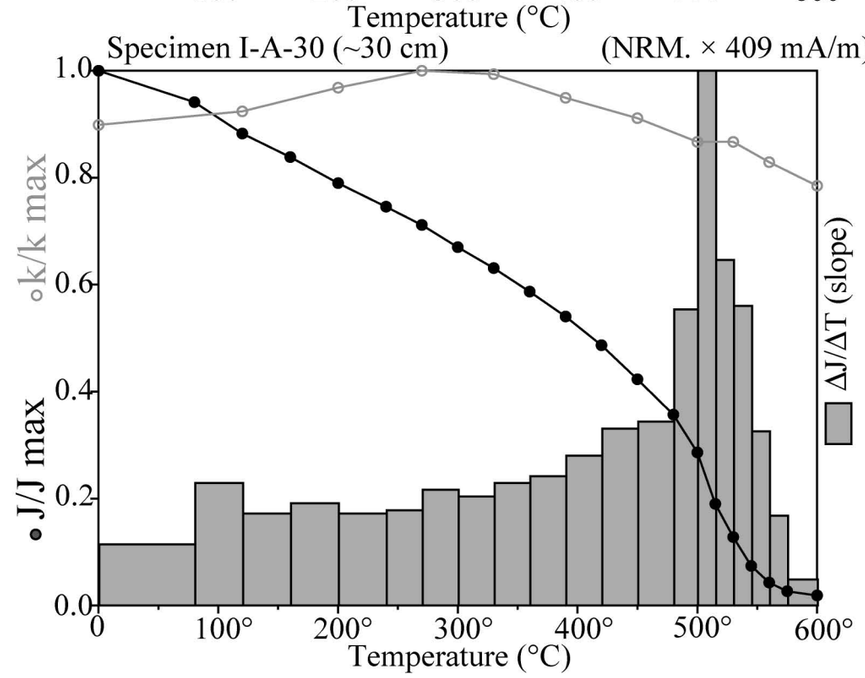
Specimen I-A-30 (~30 cm)
(NRM. × 409 mA/m)
k/k max
J/J max
ΔJ/ΔT (slope)
Temperature (°C)

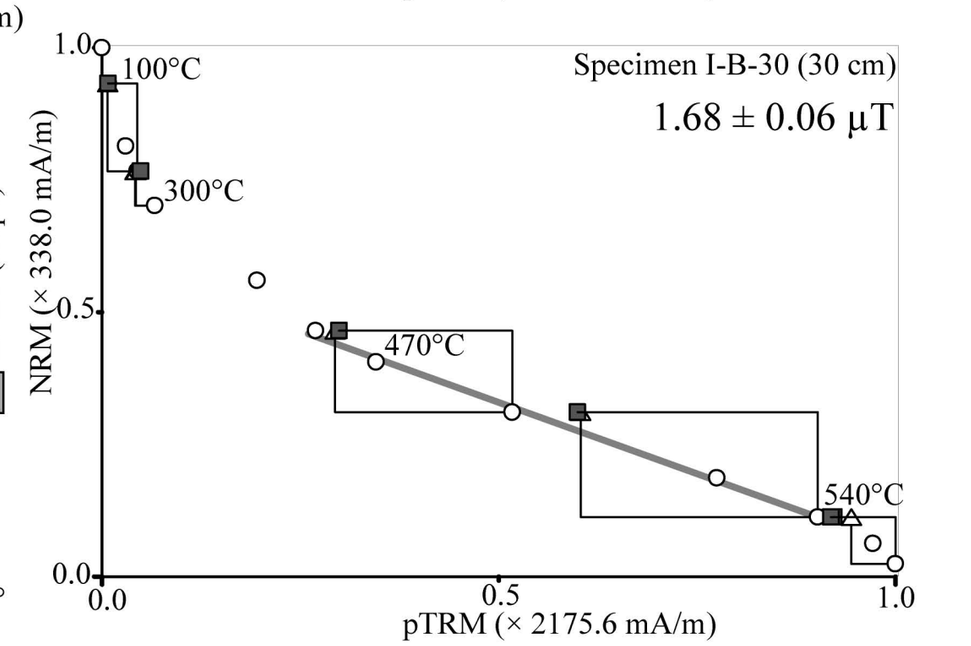
Specimen I-B-30 (30 cm)
1.68 ± 0.06 μT
100°C
300°C
470°C
540°C
NRM (× 338.0 mA/m)
pTRM (× 2175.6 mA/m)

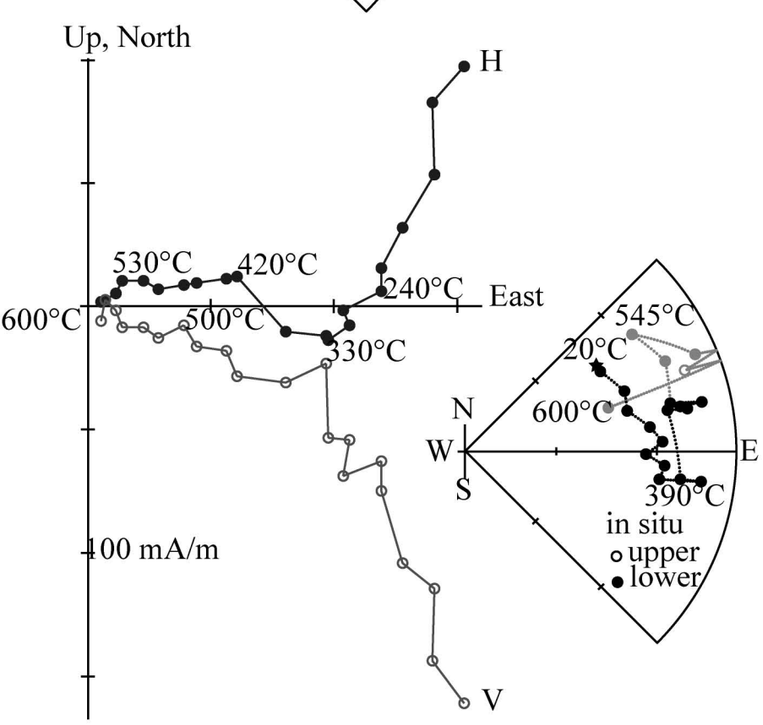
Up, North
H
530°C
420°C
240°C
East
600°C
500°C
330°C
545°C
20°C
600°C
390°C
in situ
upper
lower
N
W
E
S
100 mA/m
V

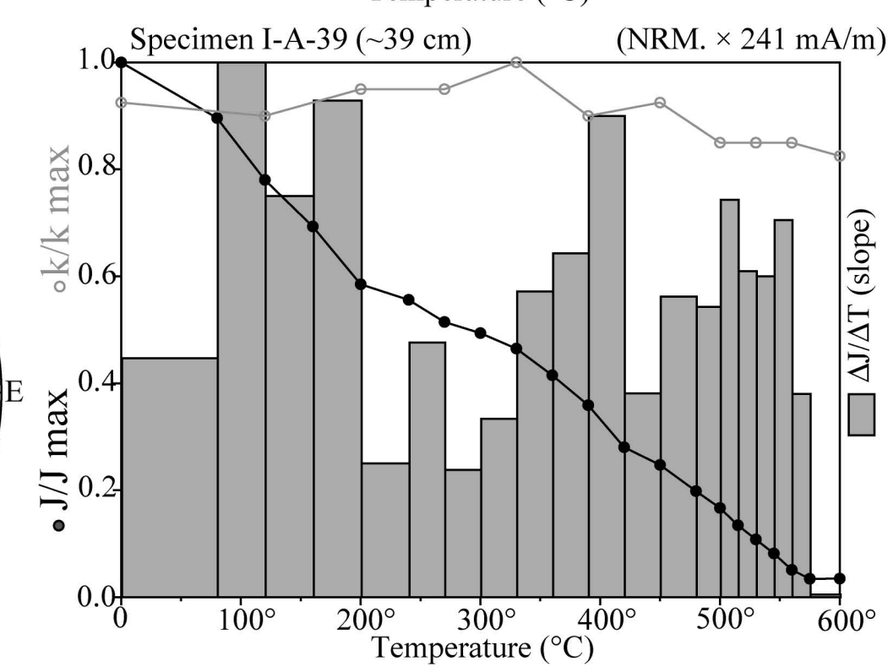
Specimen I-A-39 (~39 cm)
(NRM. × 241 mA/m)
k/k max
J/J max
ΔJ/ΔT (slope)
Temperature (°C)

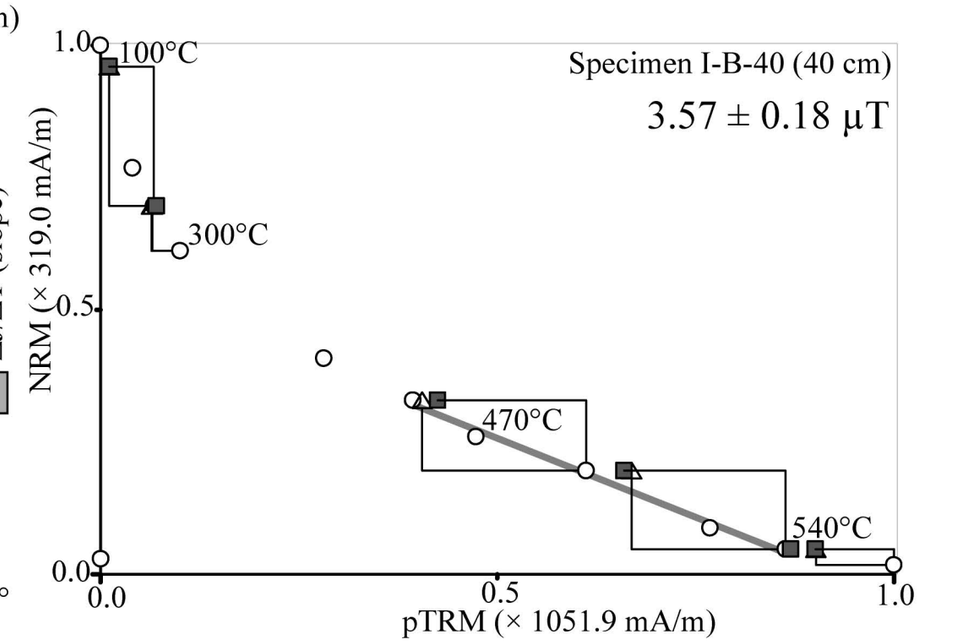
Specimen I-B-40 (40 cm)
3.57 ± 0.18 μT
100°C
300°C
470°C
540°C
NRM (× 319.0 mA/m)
pTRM (× 1051.9 mA/m)

Slab.II

B

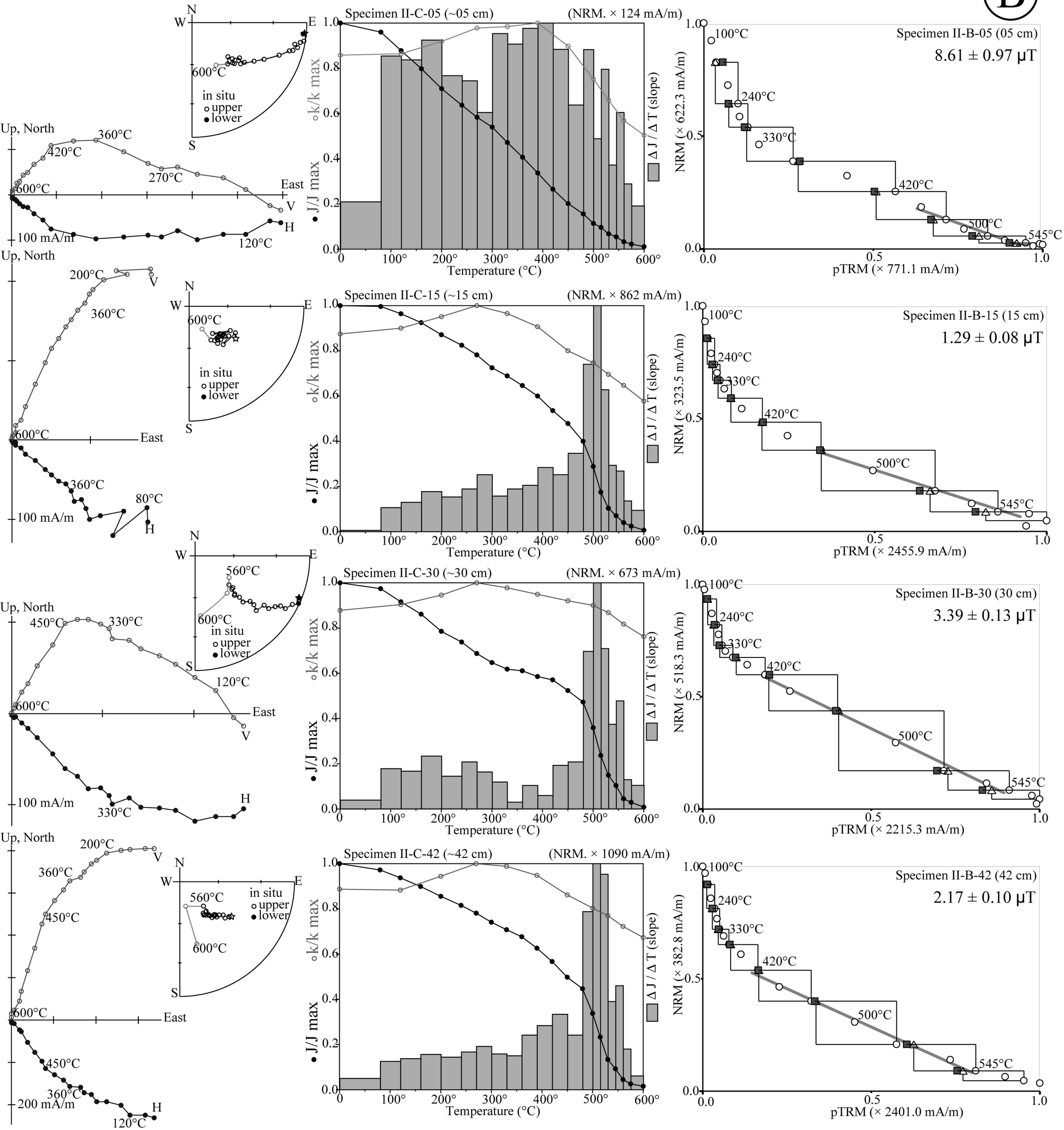
Specimen II-C-05 (~05 cm)
(NRM. × 124 mA/m)
Specimen II-B-05 (05 cm)
8.61 ± 0.97 μT
Specimen II-C-15 (~15 cm)
(NRM. × 862 mA/m)
Specimen II-B-15 (15 cm)
1.29 ± 0.08 μT
Specimen II-C-30 (~30 cm)
(NRM. × 673 mA/m)
Specimen II-B-30 (30 cm)
3.39 ± 0.13 μT
Specimen II-C-42 (~42 cm)
(NRM. × 1090 mA/m)
Specimen II-B-42 (42 cm)
2.17 ± 0.10 μT
Up, North
East
100 mA/m
200 mA/m
in situ
upper
lower
k/k max
J/J max
Δ J / Δ T (slope)
Temperature (°C)
NRM (× 622.3 mA/m)
NRM (× 323.5 mA/m)
NRM (× 518.3 mA/m)
NRM (× 382.8 mA/m)
pTRM (× 771.1 mA/m)
pTRM (× 2455.9 mA/m)
pTRM (× 2215.3 mA/m)
pTRM (× 2401.0 mA/m)

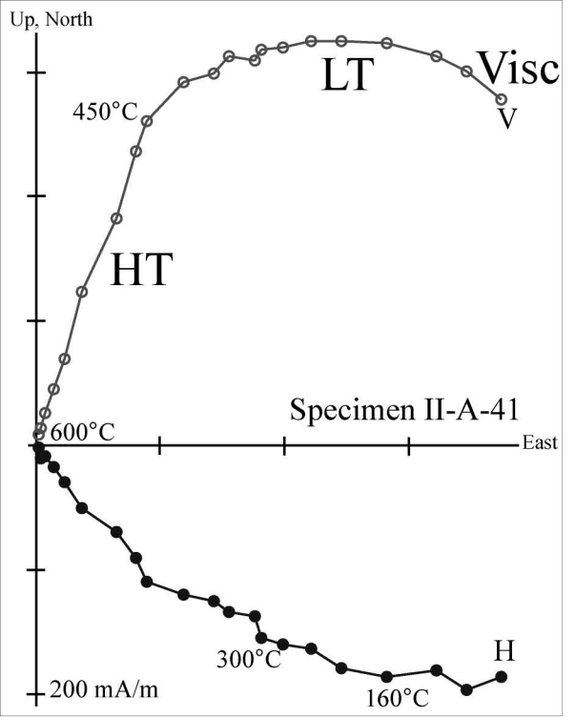

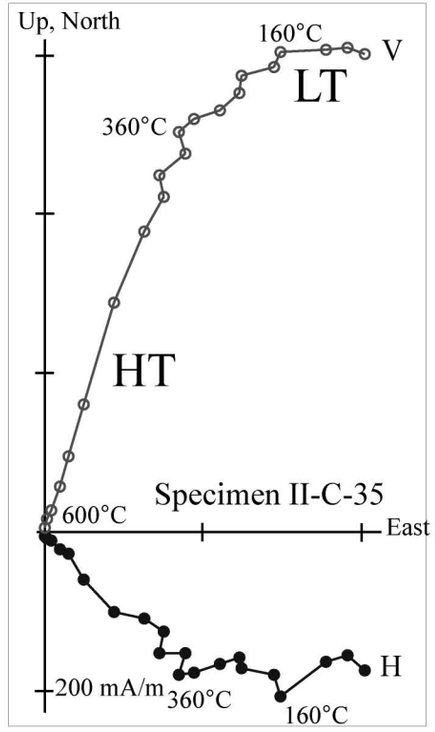

A

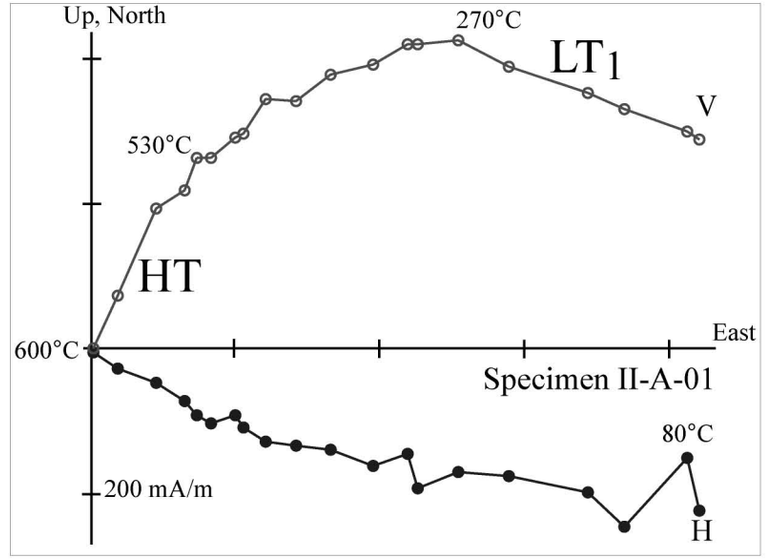

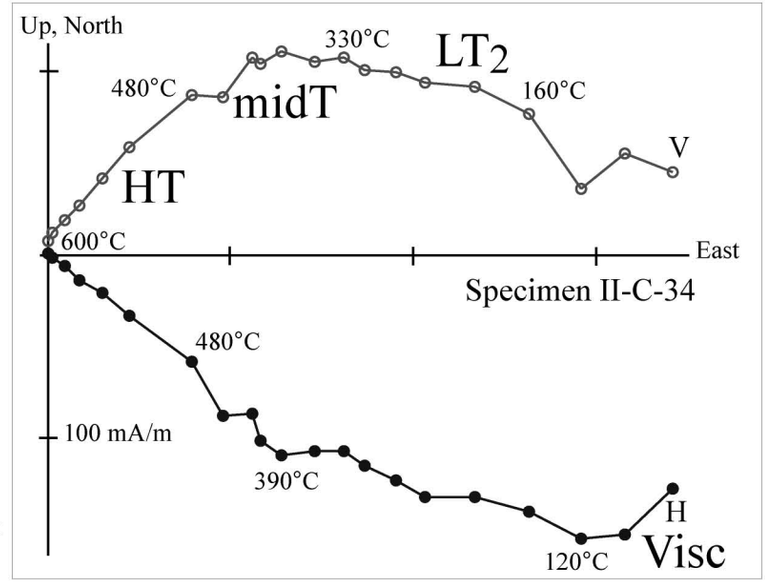

● H: projection in the horizontal plane
○ V: projection in the vertical plane

B

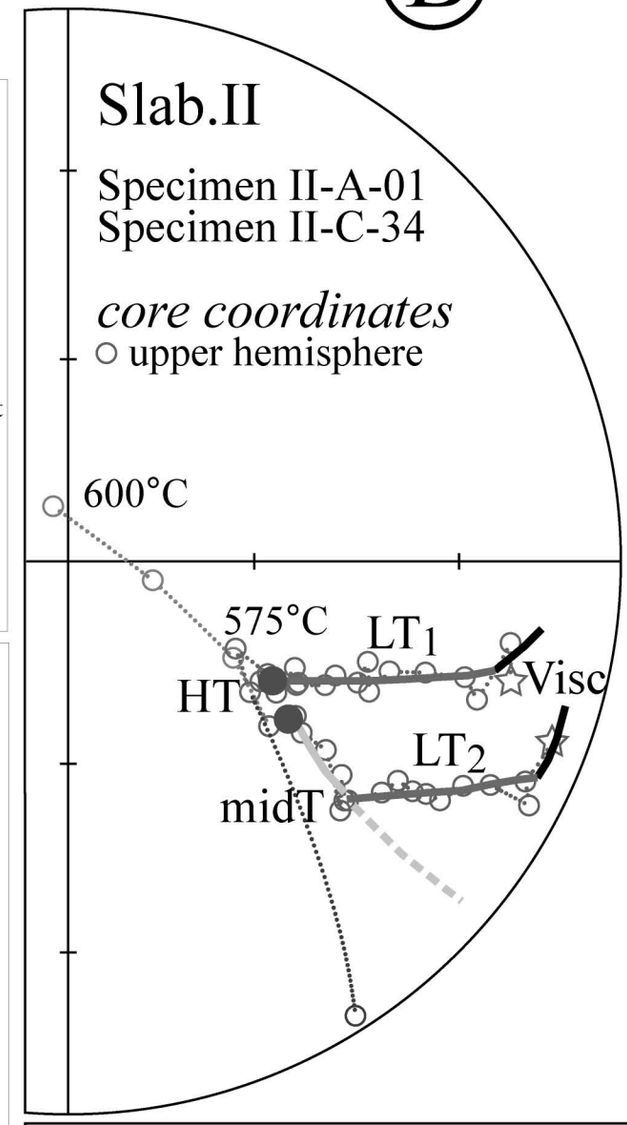

C

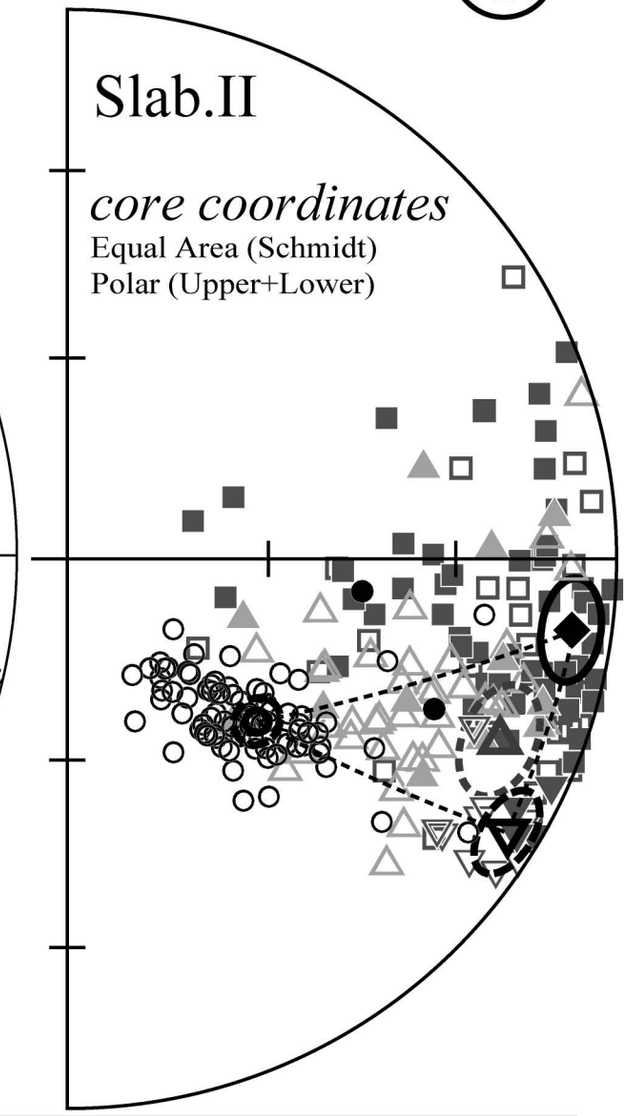

Visc: viscous magnetisation
LT: low temperature magnetisation
midT: mid temperature magnetisation
HT: high temperature magnetisation

Component	Data	Mean
LT:	■ □	◆
midT (all others):	▲ △	◬
midT, “well-isolated”:	▼ ▽	⊽
HT:	● ○	⊙

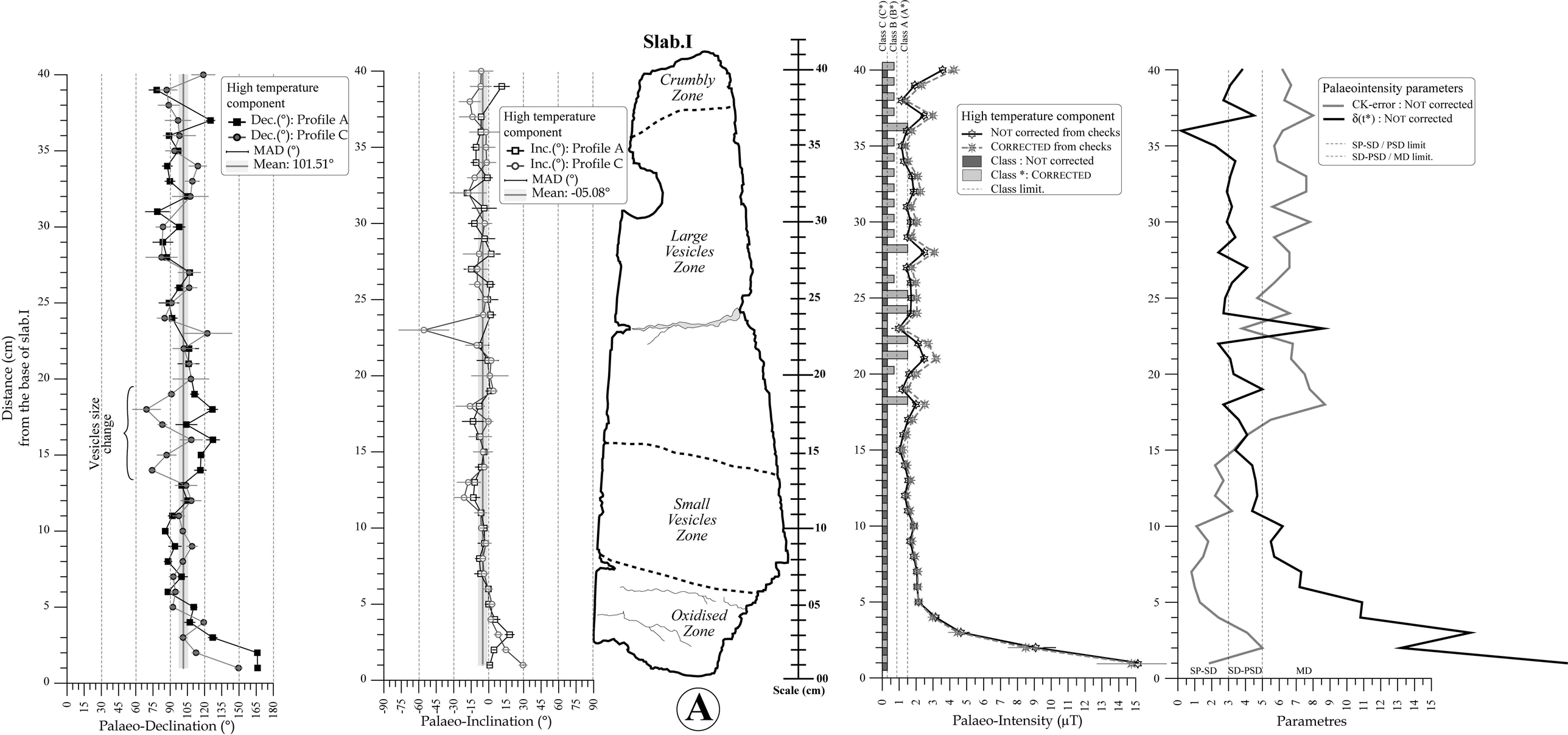
Slab.I
Distance (cm) from the base of slab.I
Vesicles size change
High temperature component
Dec.(°): Profile A
Dec.(°): Profile C
MAD (°)
Mean: 101.51°
Palaeo-Declination (°)
High temperature component
Inc.(°): Profile A
Inc.(°): Profile C
MAD (°)
Mean: -05.08°
Palaeo-Inclination (°)
Crumbly Zone
Large Vesicles Zone
Small Vesicles Zone
Oxidised Zone
Scale (cm)
A
Class C (C*)
Class B (B*)
Class A (A*)
High temperature component
NOT corrected from checks
CORRECTED from checks
Class : NOT corrected
Class *: CORRECTED
Class limit.
Palaeo-Intensity (µT)
Palaeointensity parameters
CK-error : NOT corrected
δ(t*) : NOT corrected
SP-SD / PSD limit
SD-PSD / MD limit.
SP-SD
SD-PSD
MD
Parametres

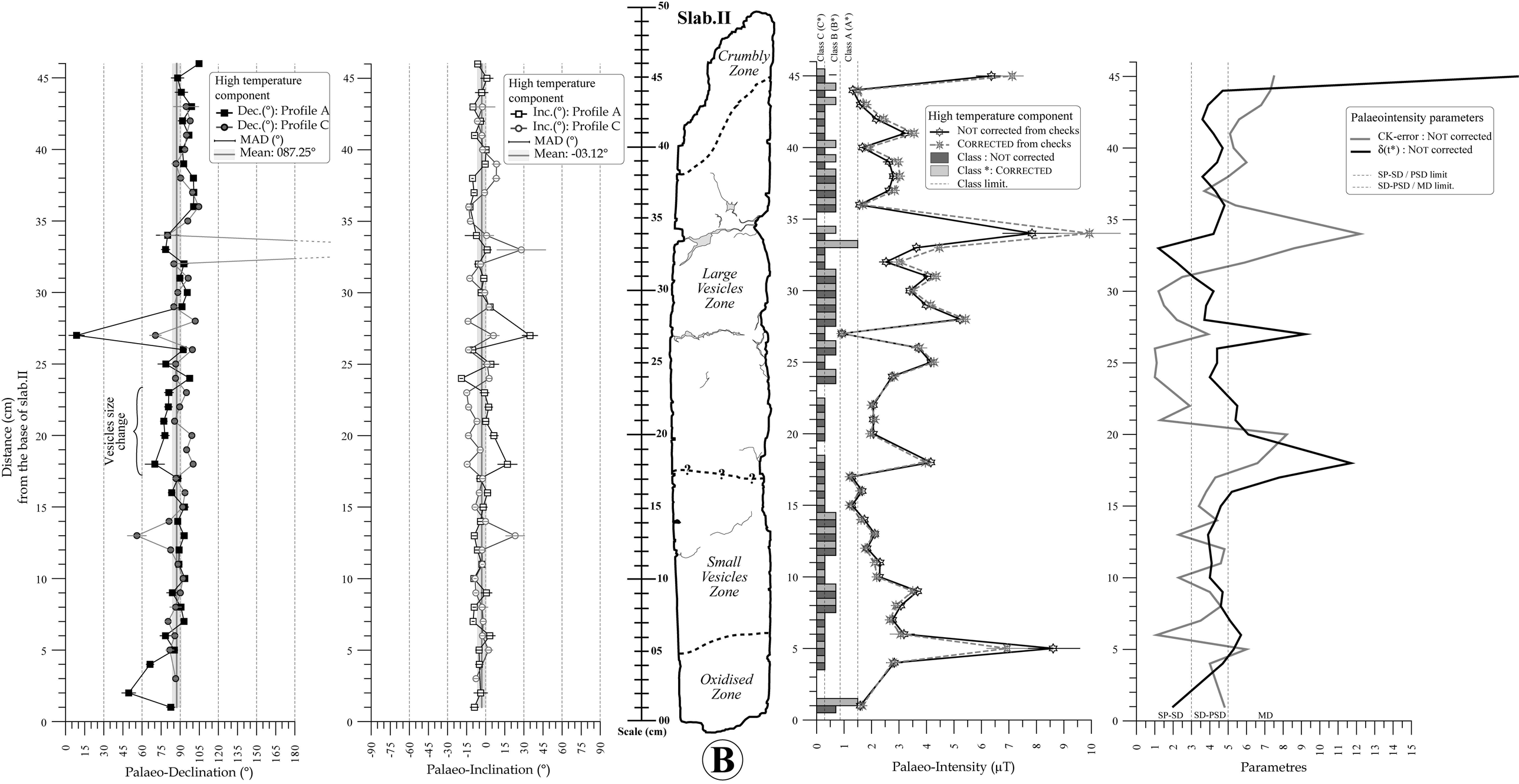
Slab.II
Distance (cm) from the base of slab.II
Vesicles size change
High temperature component
Dec.(°): Profile A
Dec.(°): Profile C
MAD (°)
Mean: 087.25°
Palaeo-Declination (°)
High temperature component
Inc.(°): Profile A
Inc.(°): Profile C
MAD (°)
Mean: -03.12°
Palaeo-Inclination (°)
Crumbly Zone
Large Vesicles Zone
Small Vesicles Zone
Oxidised Zone
Scale (cm)
B
Class C (C*)
Class B (B*)
Class A (A*)
High temperature component
NOT corrected from checks
CORRECTED from checks
Class : NOT corrected
Class *: CORRECTED
Class limit.
Palaeo-Intensity (µT)
Palaeointensity parameters
CK-error : NOT corrected
δ(t*) : NOT corrected
SP-SD / PSD limit
SD-PSD / MD limit.
SP-SD
SD-PSD
MD
Parametres

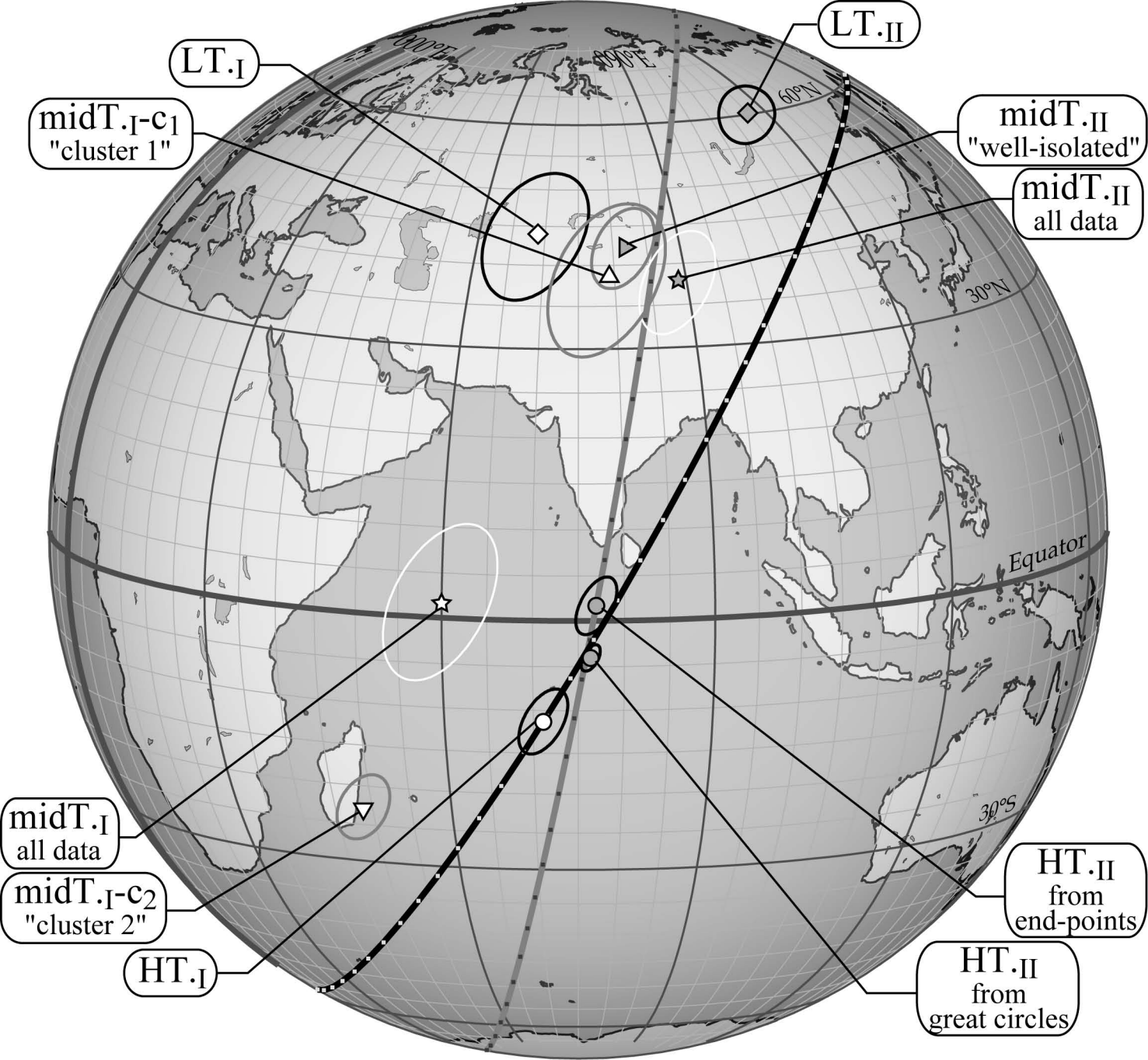
LT.II
LT.I
midT.I-c1
"cluster 1"
midT.II
"well-isolated"
midT.II
all data
60°N
30°N
Equator
30°S
midT.I
all data
midT.I-c2
"cluster 2"
HT.I
HT.II
from
end-points
HT.II
from
great circles

ACCEPTED MANUSCRIPT

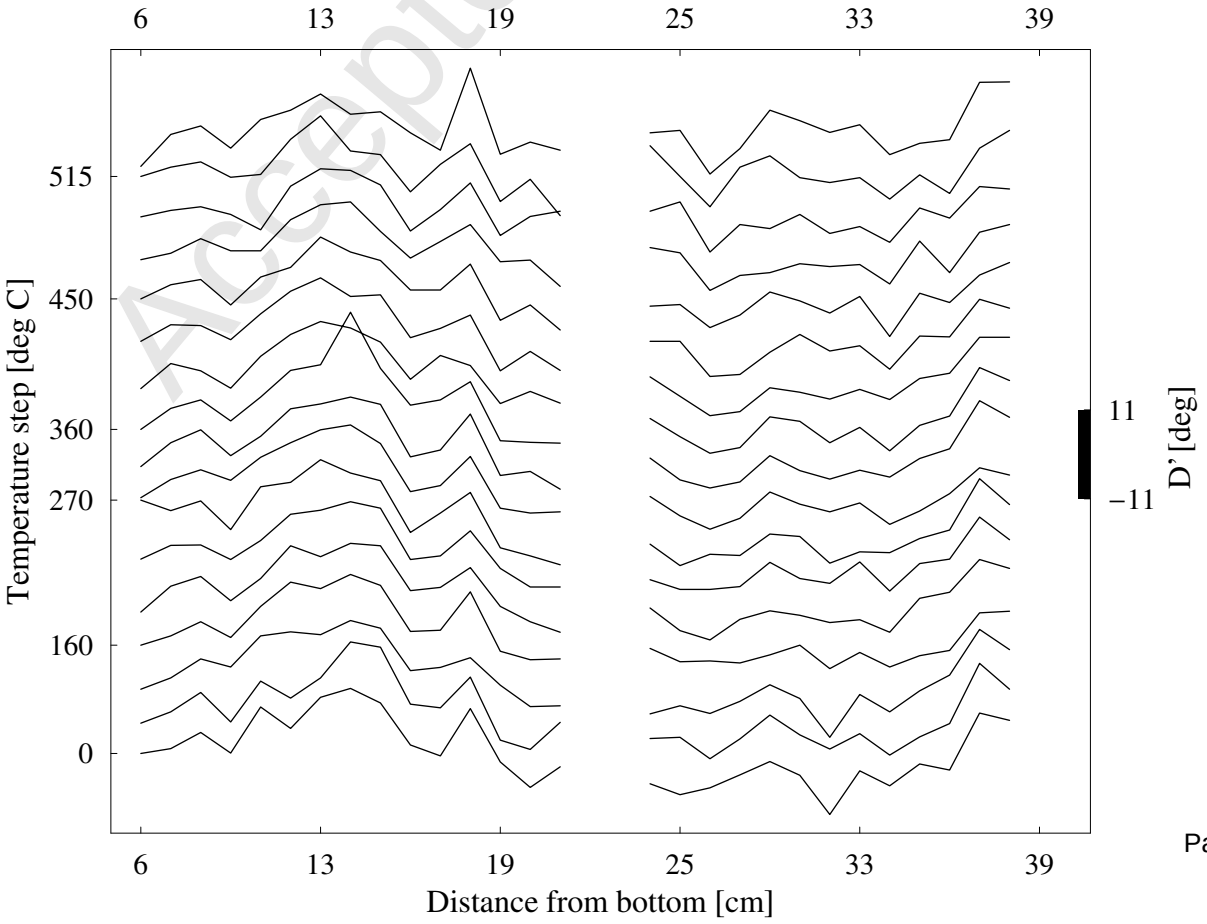

Accepted Manuscript

ACCEPTED MANUSCRIPT

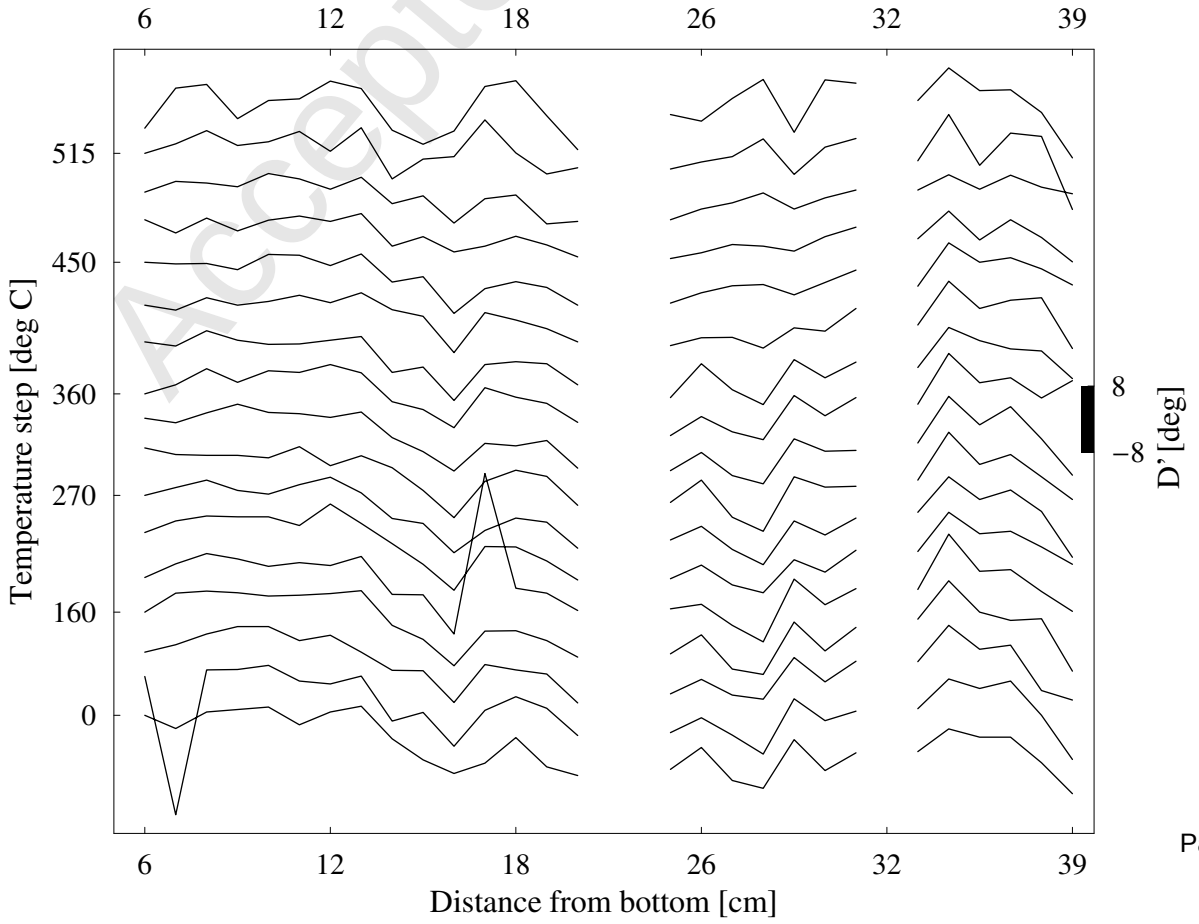

Accepted Manuscript

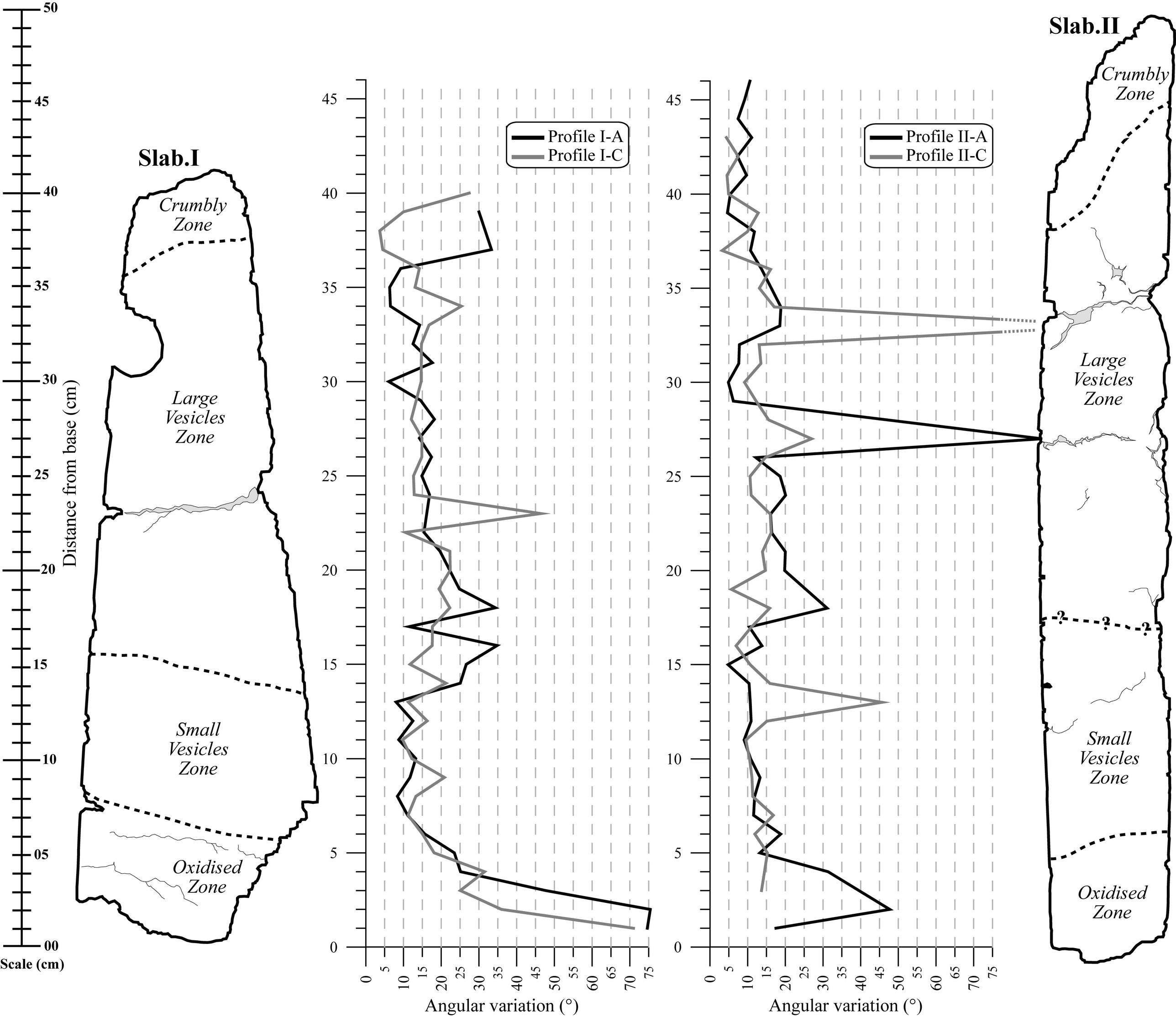
Slab.I
Crumbly Zone
Large Vesicles Zone
Small Vesicles Zone
Oxidised Zone
Distance from base (cm)
Scale (cm)
Profile I-A
Profile I-C
Angular variation (°)
Slab.II
Profile II-A
Profile II-C
Crumbly Zone
Large Vesicles Zone
Small Vesicles Zone
Oxidised Zone
Angular variation (°)